NACA TN 2685

NATIONAL ADVISORY COMMITTEE FOR AERONAUTICS

TECHNICAL NOTE 2685

A LOW-SPEED INVESTIGATION OF AN ANNULAR TRANSONIC AIR INLET

By Mark R. Nichols and Donald W. Rinkoski

Langley Aeronautical Laboratory
Langley Field, Va.

Washington
April 1952

1G

NATIONAL ADVISORY COMMITTEE FOR AERONAUTICS

TECHNICAL NOTE 2685

A LOW-SPEED INVESTIGATION OF AN ANNULAR TRANSONIC AIR INLET[1]

By Mark R. Nichols and Donald W. Rinkoski

SUMMARY

A special problem is encountered in the application of fuselage scoops to a transonic airplane in that compression shocks must be avoided on the surface of the fuselage ahead of the air inlets to prevent boundary-layer separation which would result in unstable inlet flow and losses in ram. Subsonic flow, however, can be maintained on the fuselage surface ahead of an annular inlet up to flight Mach numbers of about 1.2 and thus shocks in this region through both the subsonic and the transonic flight regions can be avoided provided that the fuselage forward of the inlet is a cone of the proper proportions. The present investigation of this type of inlet was conducted at low speeds in the Langley propeller-research tunnel in order to obtain some indication of the basic characteristics of such inlets.

Two theoretically designed cone fuselage noses of different apex angle and one ogival nose were tested in conjunction with an NACA 1-85-050 cowling which was also tested in the open-nose condition. Surface pressures and inlet total pressures were measured at the tops of the test configurations for wide ranges of inlet-velocity ratio and angle of attack.

The results of the investigation show that substream velocities were maintained on the three fuselage noses over the ranges of angle of attack and inlet-velocity ratio useful for high-speed flight. At an angle of attack of 0°, boundary-layer separation from the noses was not encountered over this range of inlet-velocity ratio. At and above its design inlet-velocity ratio, the NACA 1-85-050 cowling used as the basic inlet had approximately the same critical Mach numbers with the various noses installed as when tested in the open-nose condition; thus, data for the NACA 1-series nose inlets can be used in the design of installations of this type. At very high values of inlet-velocity ratio, the

---

[1]Supersedes the recently declassified NACA RM L6J04 entitled "A Low-Speed Investigation of an Annular Transonic Air Inlet" by Mark R. Nichols and Donald W. Rinkoski, 1947.

high negative pressure peaks encountered on the inner part of the inlet lip caused the internal flow to separate.

INTRODUCTION

The use of fuselage scoops offers several significant advantages in the arrangement of a fighter airplane: The ducting to the engine may be made as short as possible; good visibility may be obtained by locating the pilot ahead of the inlets in a thin section of the fuselage; the gun installations may be located in the nose where they will not interfere with the air inlets or ducting; and the directional stability may be improved by reducing the lateral area forward of the center of gravity.

A special problem is encountered in the application of fuselage scoops to a transonic airplane in that compression shocks must be avoided on the surface of the fuselage ahead of the air inlets to prevent boundary-layer separation which would result in unstable inlet flow and losses in ram. This condition can be fulfilled only by maintaining the velocity of the flow on this surface at subsonic values throughout the speed range of the airplane. If the fuselage forward of the inlet is a cone of the correct apex angle, it appears that the desired subsonic velocities can be maintained up to flight Mach numbers of about 1.2. Low inlet total-pressure losses can be obtained with this arrangement and the inlet lip at the base of the cone will operate essentially in a subsonic region.

Because of the great interest in these inlets and the difficulty of detailed transonic testing at adequate Reynolds numbers, a preliminary study of such designs has been made at low speeds in the Langley propeller-research tunnel. Obviously, many significant phenomena associated with compressibility were thereby not observed; however, it was considered that the study would indicate many of the basic characteristics of such inlets. In the present paper are reported studies of the pressure distributions and inlet-flow conditions for annular inlets consisting of an NACA 1-series nose inlet (reference 1) combined with two theoretically designed cone noses of different apex angle and one ogival nose, together with comparison tests of the inlet in the open-nose condition. Tests in which a canopy and wheel-well fairing were added to the test model to provide a twin-side-scoop configuration applicable to a fighter airplane are described in reference 2.

SYMBOLS

A_i	inlet area, 1.12 square feet
D	maximum diameter of cowling, 27.25 inches

h	height of inlet, 2.47 inches
H	total pressure, pounds per square foot
M_{cr}	predicted critical Mach number
p	static pressure, pounds per square foot
p_o	static pressure of free stream, pounds per square foot
q_o	dynamic pressure of free stream, pounds per square foot
u	local velocity at point in boundary layer, feet per second
U	velocity just outside boundary layer, feet per second
V_i	average velocity of flow at inlet, feet per second
V_o	velocity of free stream, feet per second
x	horizontal distance from station 0 (see fig. 2), inches
α	angle of attack of center line of model, degrees
δ	boundary-layer thickness, normal distance from surface to point where $\frac{H - p_o}{q_o} = 0.98$, inches

MODEL AND TESTS

General views of the model are shown as figure 1; line drawings of the three annular-inlet configurations and coordinates of the curved nose and of the NACA 1-85-050 nose inlet used in conjunction with each of the fuselage noses are given in figure 2. The three fuselage noses had the same maximum diameter at the inlet. The short conical nose had an apex angle of 19° and a ratio of length to diameter of about 3; whereas the long conical nose had an apex angle of 14° and a ratio of length to diameter of approximately 4. The curved nose which had approximately the same length as the short conical nose was designed to obtain increased volume within the nose; its nose angle was about 32°.

A schematic drawing of the body of the model showing the arrangement, instrumentation, and principal dimensions is presented in figure 3. The internal-flow system included an axial-flow fan which was necessary to obtain the higher inlet-velocity ratios. Flow control was obtained by varying the speed of the motor and the position of the shutters. The quantity of internal flow was measured by means of rakes of total- and static-pressure tubes at the throat of the venturi and at the exit of the model.

Surface pressures were measured by means of 11 to 15 flush orifices distributed along the top center line of each nose and 21 orifices installed in the top section of the inlet lip. Total pressures in the boundary layers of the several noses at the entrance station were measured by the use of a removable rake of nine 0.030-inch-diameter stainless-steel tubes with ends flattened to form openings about 0.005 by 0.05 inch. Pressure recoveries in the flow adjacent to the inner surface of the top section of the inlet lip were measured by means of the rake of five $\frac{1}{16}$-inch-diameter total-pressure tubes shown in figure 3. All pressures were recorded by photographing a multitube manometer.

The three annular-inlet configurations were tested over the angle-of-attack range from -2° to 6° at inlet-velocity ratios ranging from 0.4 to 1.5; whereas the open-nose cowling was investigated over the angle-of-attack range from 0° to 6° at inlet-velocity ratios ranging between 0.3 and 0.9. All tests were conducted at tunnel speeds of from 70 to 100 miles per hour; the maximum speed corresponds to a Mach number of 0.13 and a Reynolds number of about 2×10^6 based on the maximum cowling diameter.

RESULTS AND DISCUSSION

The results of the present investigation are discussed in three sections as follows: surface pressures on the noses, surface pressures on the inlet lip, and flow conditions at the inlet.

Surface pressures on noses.- Static-pressure distributions over the top external surface of the three inlet configurations are presented in figures 4 to 6.

The static-pressure distributions over the short conical-nose configuration at an angle of attack of 0° (fig. 4(b)) show that substream velocities were obtained over the entire nose for low and medium values of inlet-velocity ratio. The effect of increasing the inlet-velocity ratio was to raise the velocities on the surface of the nose; however, these increases were very small except within one-half cowling diameter

ahead of the inlet. Superstream velocities occurred at the inlet at inlet-velocity ratios above approximately 0.9. The surface pressure on the nose at the inlet was always more negative than the corresponding value that could be estimated from the inlet-velocity ratio because the inlet-velocity distribution was nonuniform due to the boundary layer on the nose and to the pressure field of the inlet lip.

The more significant effect of increasing the angle of attack of the model with the short conical nose was to increase (at the top of the nose) the extent of the superstream velocity field ahead of the inlet for inlet-velocity ratios above approximately 1.1. Small decreases were effected in the local velocities on the top of the nose at the inlet; presumably, as indicated by the data for the top of the nose at $\alpha = -2^{\circ}$, corresponding small increases were effected in the local velocities at the bottom of the nose.

Velocities over the forward part of the long conical nose, although substream, were slightly higher than those for the short conical nose. (Compare figs. 4 and 5.) This condition caused some increases in the extent of the superstream velocity fields ahead of the inlet for the higher inlet-velocity ratios. At values of inlet-velocity ratio below unity, however, conditions at the section immediately in front of the inlet were essentially the same as those for the short nose.

The introduction of curvature to the sides of the short nose caused decreases in the surface velocities well forward on the nose but also resulted in the formation of a minimum pressure peak located 0.5 to 1.0 cowling diameters ahead of the inlet. (Compare figs. 4 and 6.) The surface velocities in the latter region were approximately free-stream values at an inlet-velocity ratio of 0.9 at an angle of attack of 0°. At the usual high-speed inlet-velocity ratios, however, superstream velocities did not occur within the useful range of angle of attack. Surface velocities at the inlet of the curved-nose configuration, in general, were slightly lower than those for the conical-nose configuration at any given value of inlet-velocity ratio, probably because of the improved alinement of the entering flow.

The following table presents the maximum values of inlet-velocity ratio for which substream velocities were maintained on the three noses at angles of attack of 0° and 2°:

Nose	$\alpha = 0^{\circ}$	$\alpha = 2^{\circ}$
Short cone	0.88	0.83
Long cone	.93	.87
Curved	.91	.73

For $\alpha = 2^\circ$, the preceding maximum values were determined in the case of the two conical noses by the pressures on the bottom surfaces at the inlet, and in the case of the curved nose by the pressures on the top surface of the nose well forward of the inlet. These velocity ratios exceed the usual design values for high-speed flight and thus indicate the feasibility of this type of inlet for a transonic airplane. The critical Mach number characteristics of the top surfaces of the three noses (predicted by the use of the von Kármán relationship (reference 3) and qualified by the fact that some of the higher inlet-velocity ratios are unobtainable in the high-speed flight conditions due to choking of the inlet) are presented in figure 7 for the range of inlet-velocity ratio over which superstream surface velocities occurred.

Surface pressures on inlet lip.- The pressure distributions over the external surface of the lip of the annular inlets (figs. 4 to 6) were essentially similar to those for the basic open-nose cowling (fig. 8), and were characteristic of those for the NACA 1-series nose inlets in that they were fairly flat at and above the inlet-velocity ratios which were required to prevent the occurrence of a negative pressure peak at the leading edge. The predicted critical Mach number characteristics for this surface are shown in figure 7 as a function of the inlet-velocity ratio for angles of attack of 0° and 4° and are compared in figure 9 at $\alpha = 0^\circ$ with corresponding data for the NACA 1-85-050 open-nose cowling. This comparison shows that at and above its design inlet-velocity ratio (that is, beyond the knee of the curve) the basic inlet had approximately the same critical Mach numbers with the various noses installed as when tested in the open-nose condition. Below the design point, the critical speeds for the lip of the annular-inlet configurations decreased more gradually with decreases in the inlet-velocity ratio than did those for the open-nose cowling, probably because the presence of the noses improved the alinement of the entering flow. (See fig. 8.) The curved nose produced a higher critical speed of the inlet lip than did the conical noses over most of the range of V_i/V_o for the same reason. The flow appears to have been separated from the lip of the open-nose cowling at $\frac{V_i}{V_o} = 0.3$ because of the high effective angle of attack of the lip.

The foregoing results indicate that satisfactory lips for this type of inlet can be designed by application of existing data for the NACA 1-series nose inlets; the design charts of reference 1 cover the selection of these inlets for critical Mach numbers as high as 0.9. In the use of these data it should be noted that the critical Mach number is defined as the Mach number at which sonic velocity is attained on the surface of the nose inlet. Tests of airfoils and streamlined bodies indicate that the Mach number at which shock separation and abrupt drag increases take place is somewhat greater than the critical Mach number.

Static-pressure distributions around the top section of the inlet lip (fig. 10) show that negative pressure coefficients occurred on the inside of the lip at inlet-velocity ratios above 0.9 at an angle of attack of 0°. Both decreases in α and further increase in V_i/V_o caused rapid increases in the values of these negative pressure coefficients; the internal flow therefore might be expected to separate from the lower lip of the inlet in the climb condition in which combinations of high values of V_i/V_o and α are encountered. This result, together with the fact that the critical Mach numbers for this surface were lower than those for any other component of the inlet at high values of V_i/V_o (fig. 7), stresses the necessity for the experimental development of less sensitive inner-lip fairings.

Flow conditions at inlet.- Total-pressure and velocity distributions in the boundary layers of the three noses at the inlet are presented in figures 11 and 12, respectively. The profiles are typical of those for turbulent flow. Decreases in the inlet-velocity ratio caused rapid increases in boundary-layer thickness because of the resulting increases in the adverse pressure gradient in front of the inlet. Extensive pressure fluctuations at the recording manometer furnished an indication that the boundary layers on the three noses were unstable at $\frac{V_i}{V_o} = 0.4$; the sample total-pressure and velocity profiles given in figures 11 and 12 show that the flow was either separated or on the verge of separation from the surface of the two conical noses for this test condition.

The boundary-layer thickness δ and the ratio of this thickness to the inlet height δ/h are presented in figure 13 as a function of the inlet-velocity ratio. The boundary-layer thicknesses for the short conical nose and the curved nose were of the same order over most of the V_i/V_o range and were about 19 percent of the inlet height for a typical high-speed inlet-velocity ratio of 0.7 compared to about 32 percent for the long conical nose. As the high-speed inlet-velocity ratio for an installation of this type probably would not be less than 0.6, the boundary-layer instability and flow separation mentioned in the preceding paragraph probably would not be encountered except in the dive condition with the engine throttled.

Total-pressure recoveries in the outer half of the inlet annulus at the top of the model are shown in figure 14. The losses for low inlet-velocity ratios, which increased rapidly with angle of attack, were caused by the separated boundary layer on the noses. (See fig. 11 for inner part of boundary-layer profiles for $\alpha = 0°$.) The losses for high inlet-velocity ratios and low angles of attack were caused by separation of the flow from the inner fairing of the lip due to the negative pressure peaks shown in figure 10. Since separation from the lip at the

bottom of the inlet would be especially severe in the climb condition, this result again stresses the necessity for further development of inner-lip fairings for use at inlet-velocity ratios greater than unity. For angles of attack between -2° and 2°, the flow did not separate from either the inlet lip or the noses of the three configurations for inlet-velocity ratios between 0.7 and 1.0. The short conical nose appeared to have a somewhat wider separation-free operating range of inlet-velocity ratio than did the other two noses.

SUMMARY OF RESULTS

A low-speed investigation has been made of three transonic fuselage-inlet installations designed to maintain substream velocities on the body ahead of the air inlets. The more significant results and conclusions of this investigation are summarized as follows:

1. Substream velocities were maintained on the three cone fuselage noses over the ranges of angle of attack and inlet-velocity ratio useful for high-speed flight.

2. The thicknesses of the boundary layers on the short and long noses were about 19 and 32 percent of the inlet height, respectively, for a typical high-speed inlet-velocity ratio of 0.7. Boundary-layer separation was not encountered at an angle of attack of 0° over the range of inlet-velocity ratio useful for high-speed flight.

3. At and above its design inlet-velocity ratio, the NACA 1-85-050 cowling used as the basic inlet had approximately the same critical Mach numbers with the various noses installed as when tested in the open-nose condition. Below this design point, the critical speeds for the inlet lip of the annular-inlet configurations decreased more gradually with decreases in inlet-velocity ratio than did those for the basic cowling. Thus, data for the NACA 1-series nose inlets, which cover the range of critical Mach number up to 0.9, can be used in the design of installations of this type.

4. At very high values of inlet-velocity ratio the high negative pressure peaks encountered on the inner part of the inlet lip caused the internal flow to separate. This result stresses the necessity for

the development of less sensitive inner-lip fairings for inlets which operate at inlet-velocity ratios exceeding unity.

Langley Aeronautical Laboratory
National Advisory Committee for Aeronautics
Langley Field, Va., October 11, 1946

REFERENCES

1. Baals, Donald D., Smith, Norman F., and Wright, John B.: The Development and Application of High-Critical-Speed Nose Inlets. NACA Rep. 920, 1948. (Supersedes NACA ACR L5F30a.)

2. Nichols, Mark R., and Goral, Edwin B.: A Low-Speed Investigation of a Fuselage-Side Air Inlet for Use at Transonic Flight Speeds. NACA TN 2684, 1952. (Supersedes NACA RM L7A06.)

3. Von Kármán, Th.: Compressibility Effects in Aerodynamics. Jour. Aero. Sci., vol. 8, no. 9, July 1941, pp. 337-356.

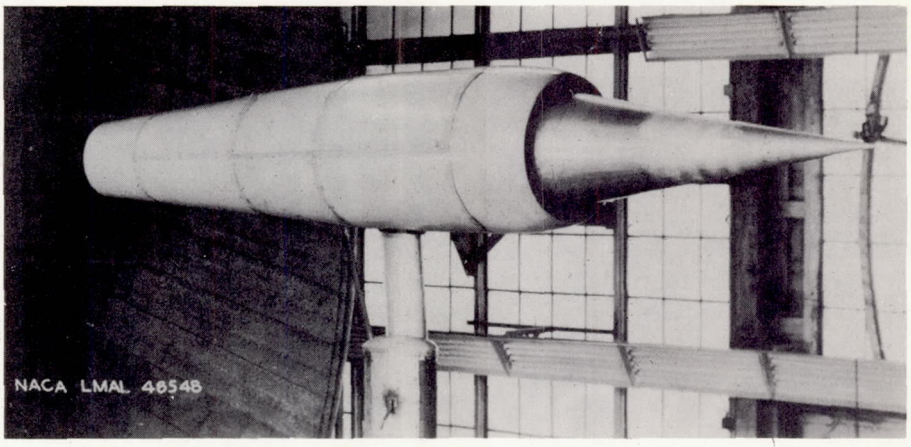

(a) Short conical nose.

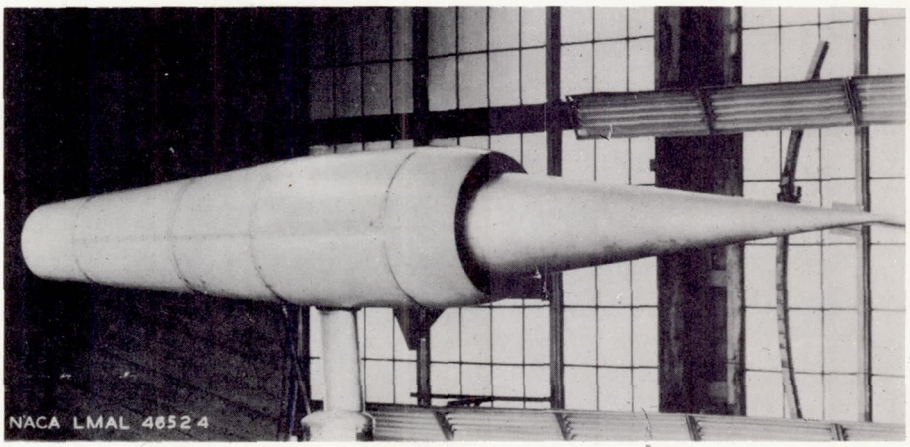

(b) Long conical nose.

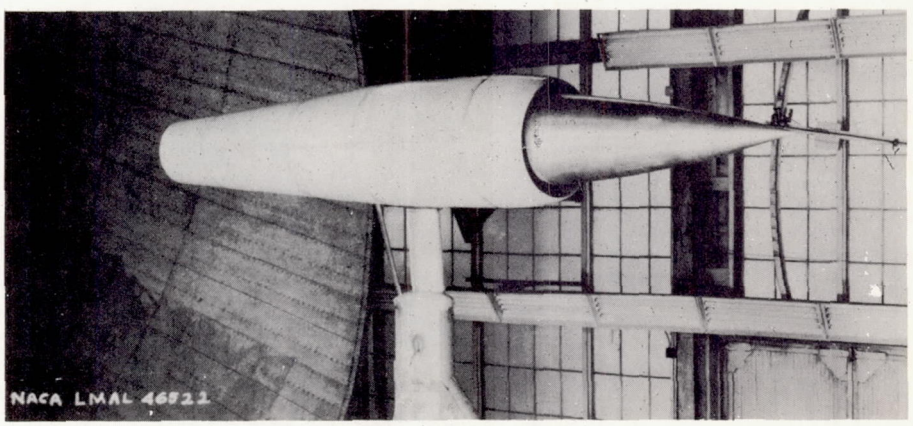

(c) Curved nose.

Figure 1.- General views of the model with the three annular inlet configurations.

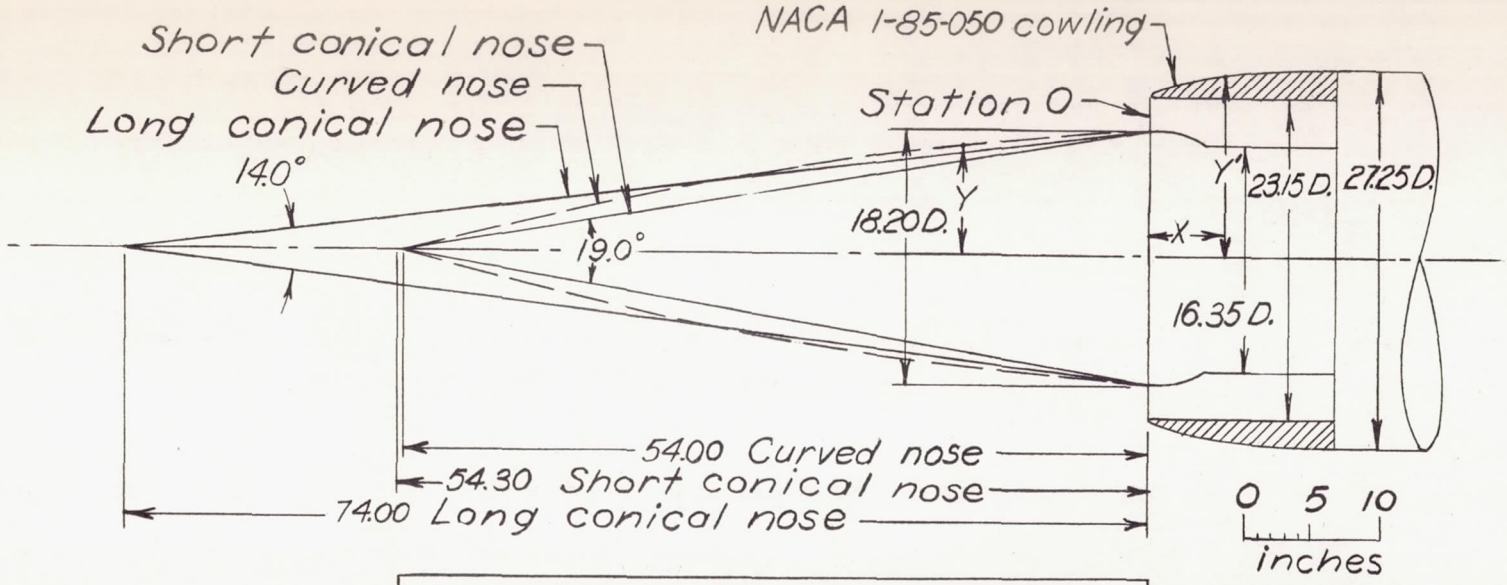

Coordinates of Curved Nose and Cowling								
X	Y	X	Y	Y'	X	Y'	X	Y'
-54.00	0	-2.50	8.90	-----	1.23	12.30	8.17	13.40
-52.00	.57	0	9.10	11.62	1.36	12.34	8.85	13.45
-50.00	1.09	.03	----	11.72	1.70	12.44	9.53	13.50
-47.50	1.69	.08	----	11.78	2.04	12.52	10.22	13.53
-45.00	2.29	.14	----	11.83	2.38	12.60	10.90	13.56
-40.00	3.42	.20	----	11.87	2.72	12.67	11.58	13.58
-35.00	4.49	.27	----	11.91	3.41	12.80	12.26	13.60
-30.00	5.47	.41	----	11.98	4.09	12.91	12.94	13.62
-25.00	6.33	.54	----	12.05	4.77	13.02	13.62	13.62
-20.00	7.07	.68	----	12.11	5.45	13.11	L.E. Rad.	
-15.00	7.71	.82	----	12.16	6.13	13.20	of Cowling	
-10.00	8.23	.95	----	12.21	6.81	13.27	0.05	
-5.00	8.70	1.09	----	12.25	7.49	13.34		

Figure 2.- Arrangement and dimensions of several annular inlet configurations. All dimensions are in inches.

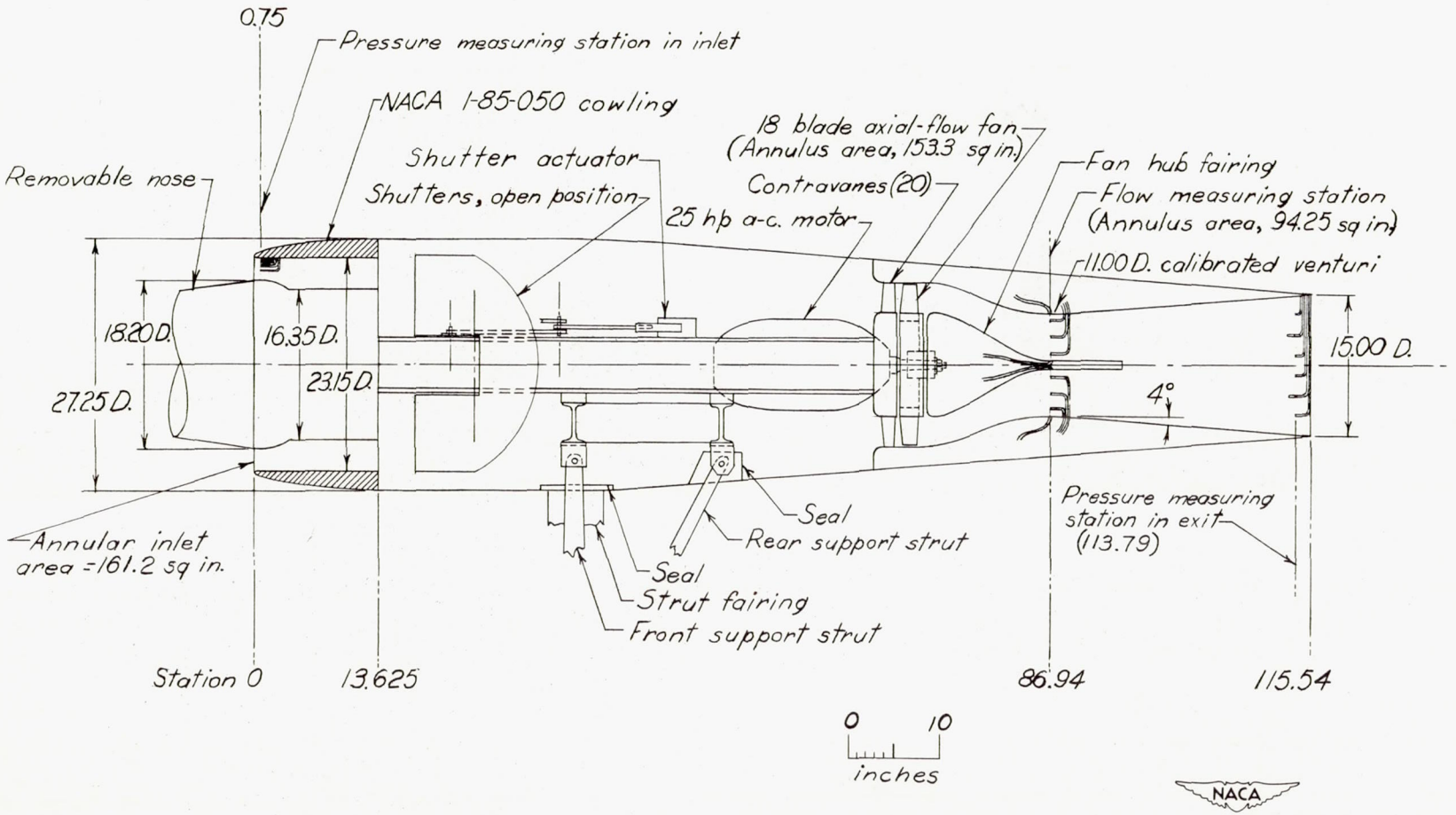

Figure 3.- Schematic drawing of body of model showing the arrangement, instrumentation, and principal dimensions. All dimensions are in inches.

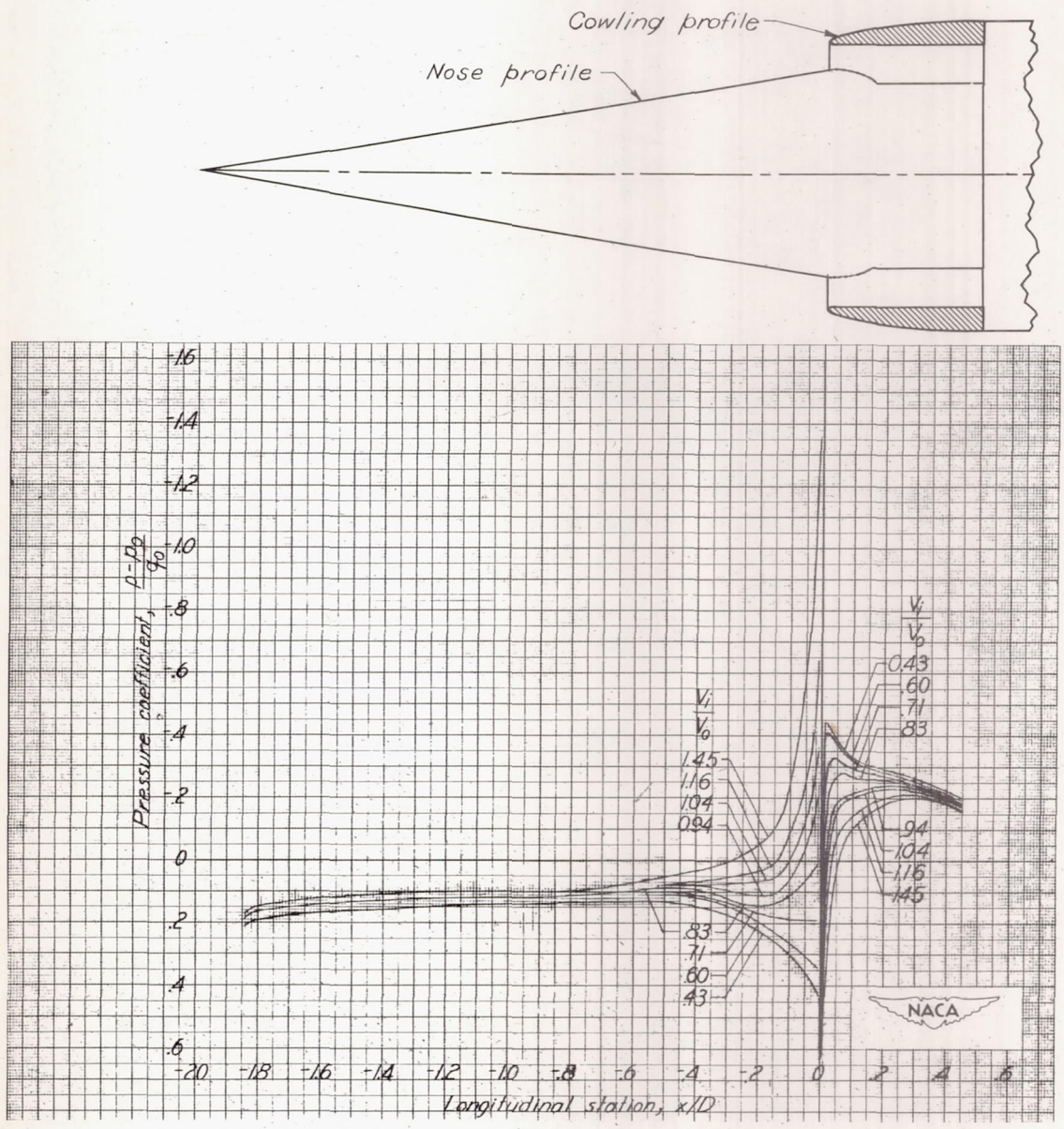

(a) $\alpha = -2^\circ$.

Figure 4.- Static-pressure distributions over top external surface of model with short conical nose installed.

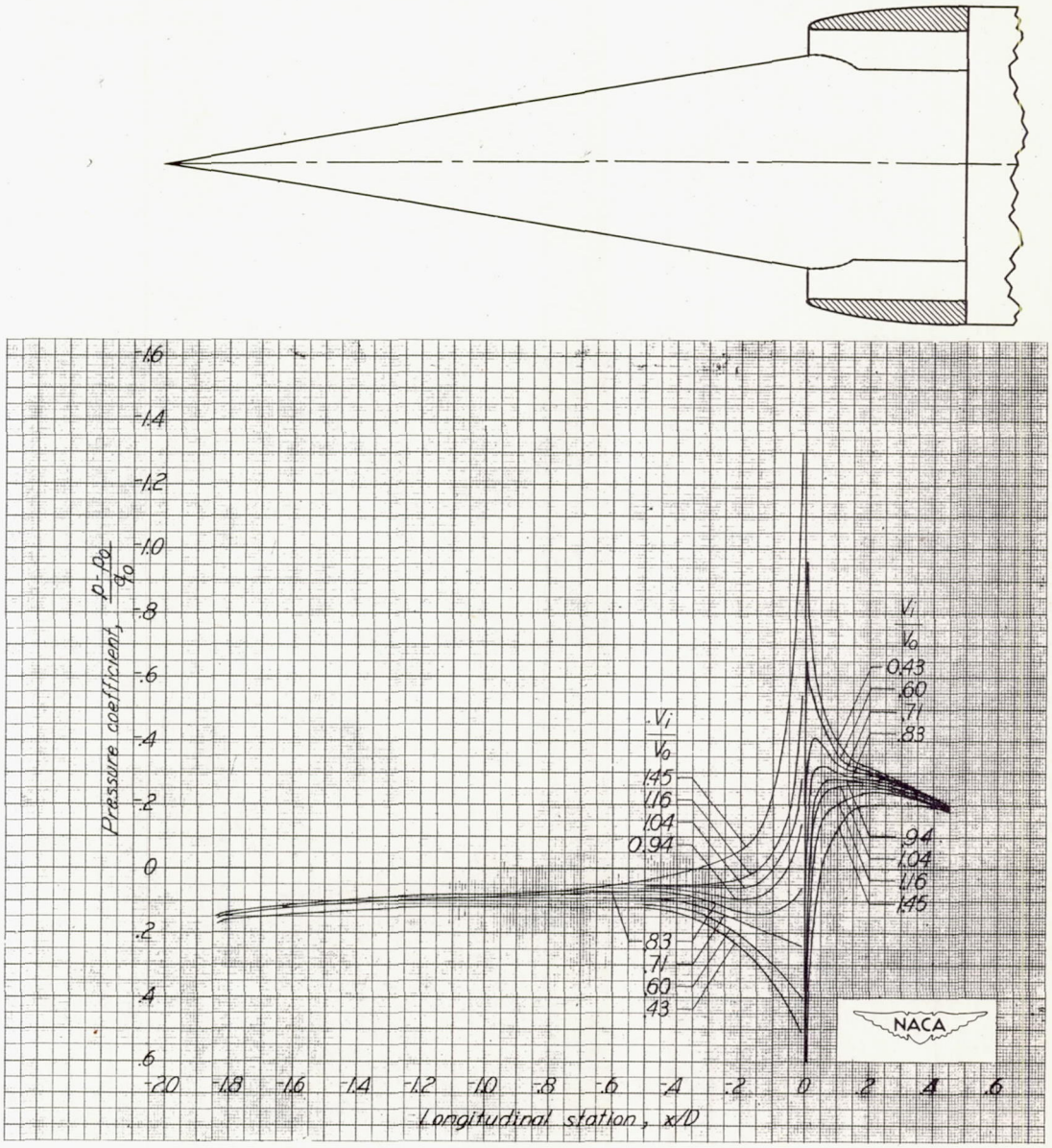

(b) $\alpha = 0^{\circ}$.

Figure 4.- Continued.

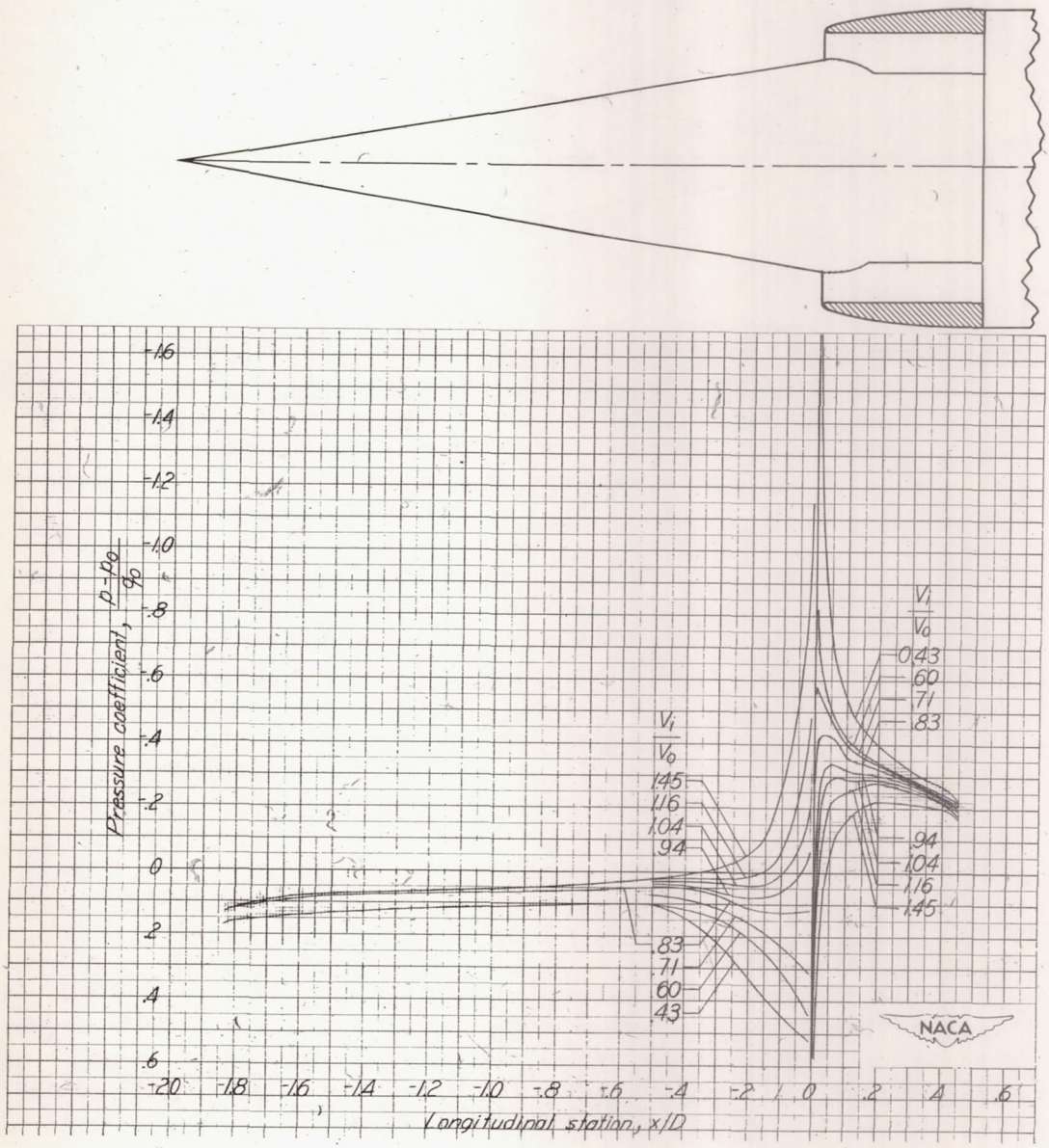

(c) $\alpha = 2^{\circ}$.

Figure 4.- Continued.

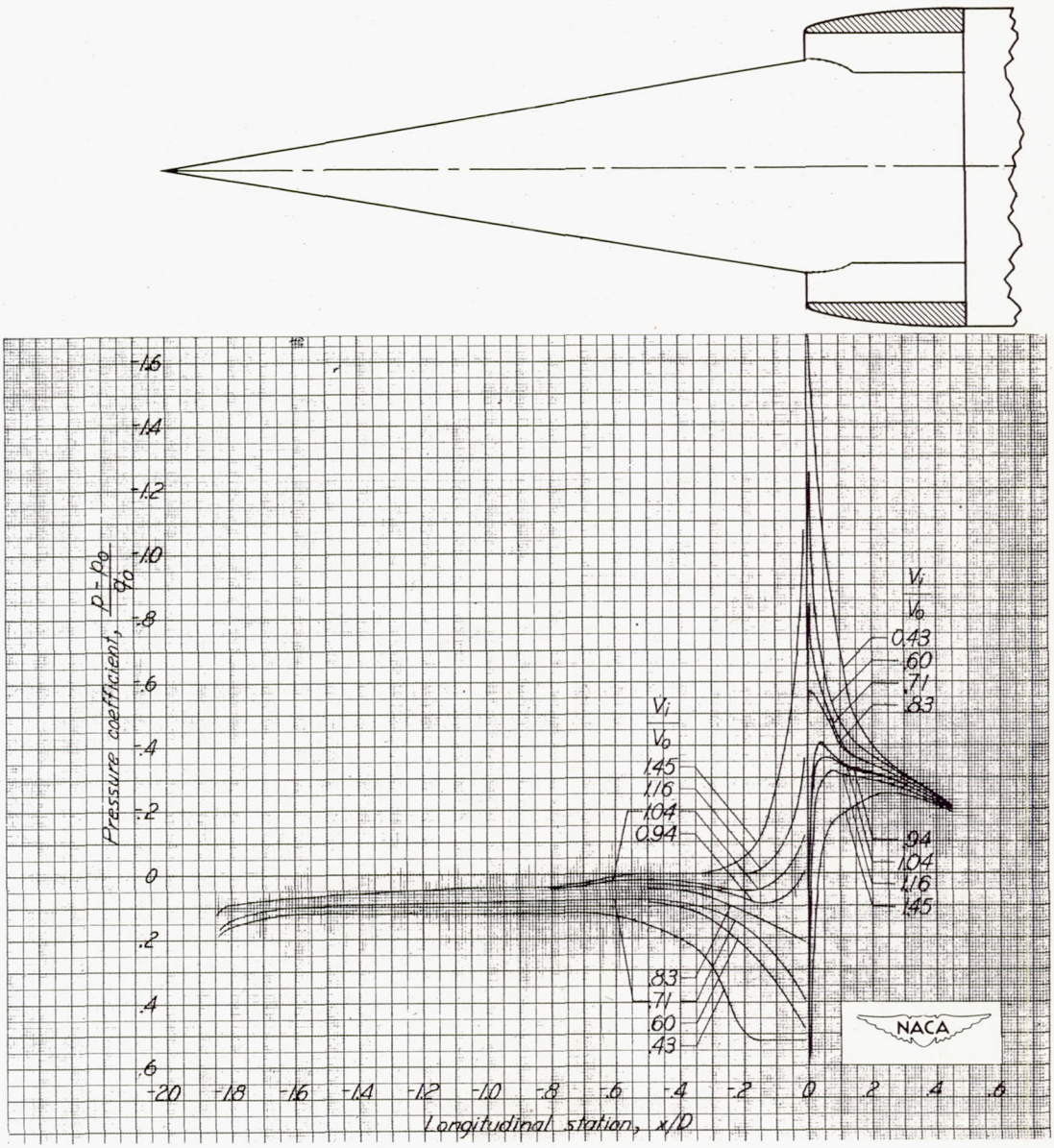

(d) $\alpha = 4^{\circ}$.

Figure 4.- Continued.

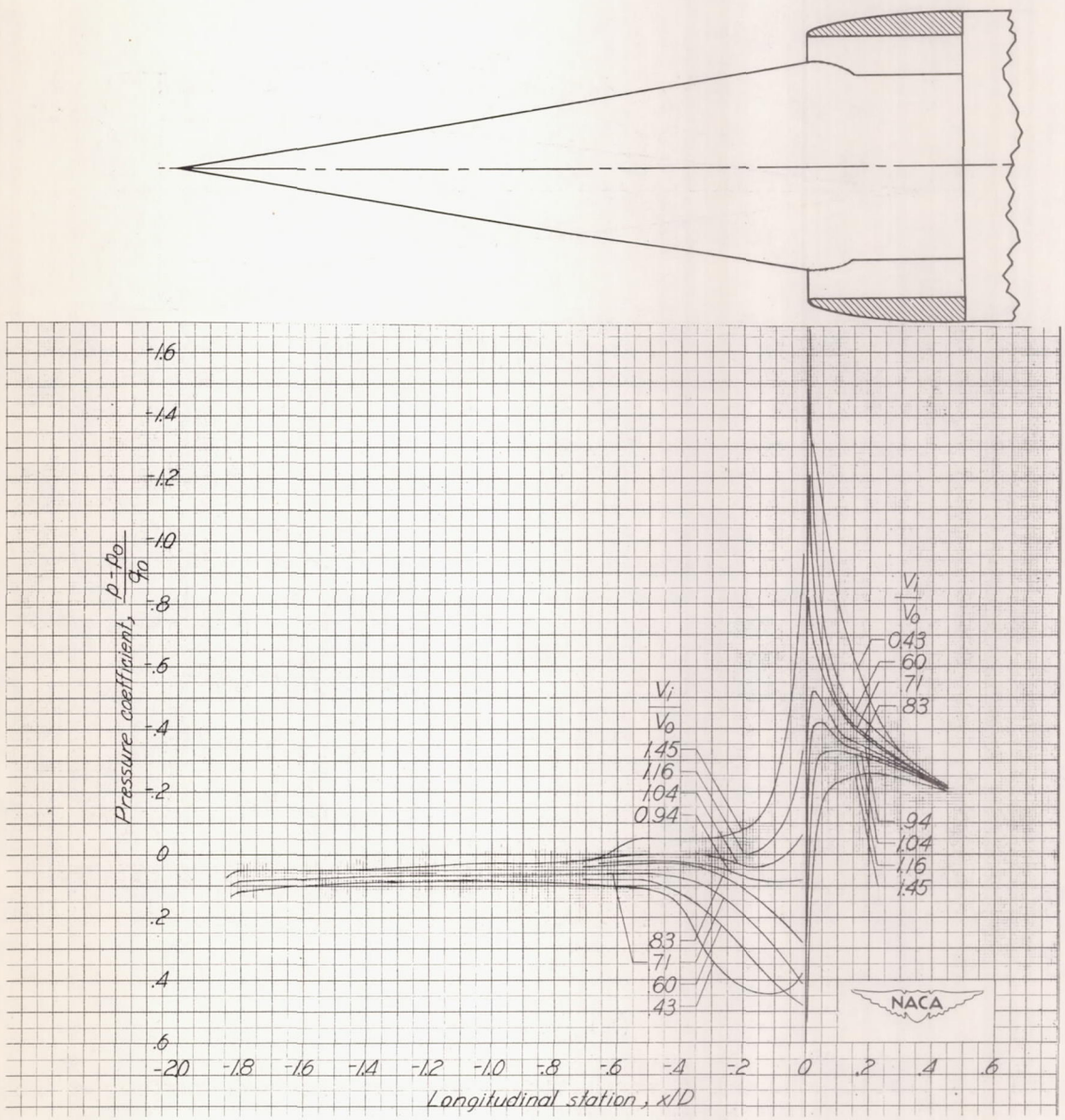

(e) $\alpha = 6^\circ$.

Figure 4.- Concluded.

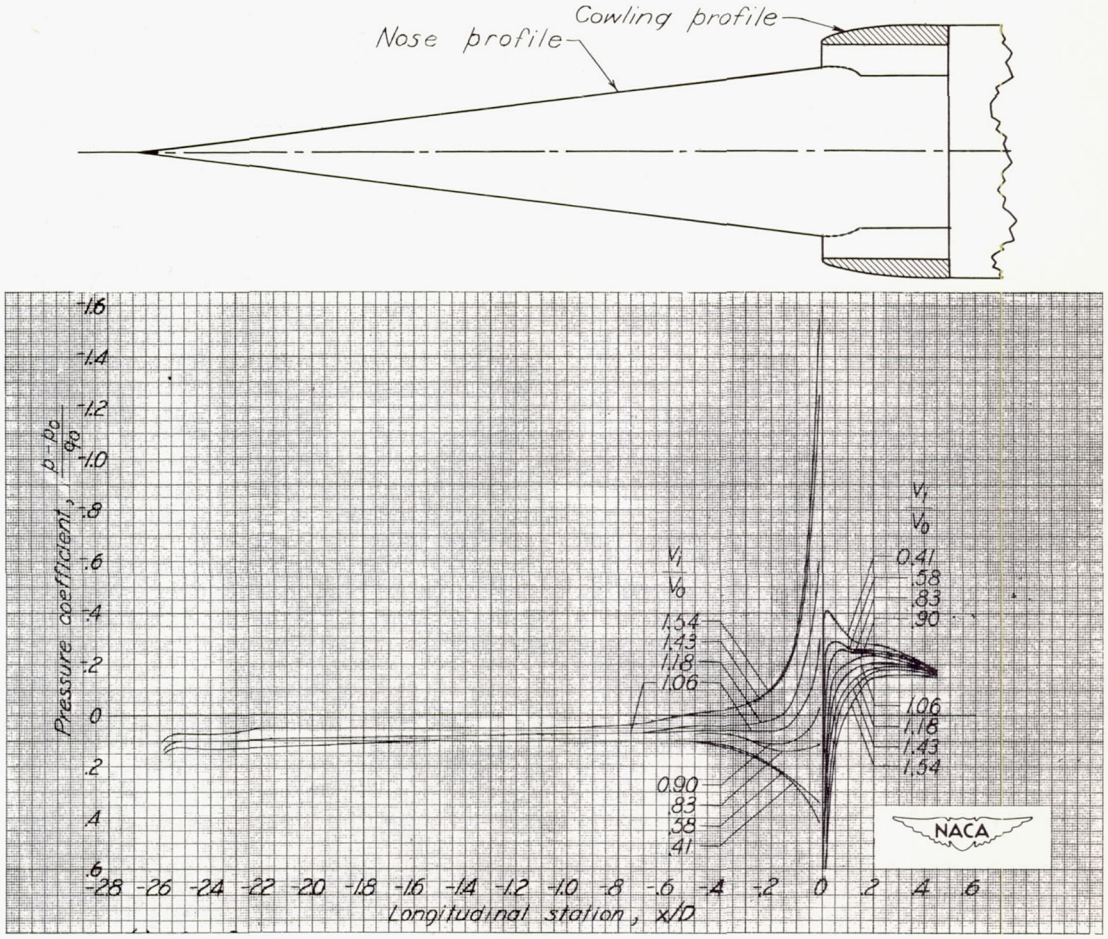

(a) $\alpha = -2^{\circ}$.

Figure 5.- Static-pressure distributions over top external surface of model with long conical nose installed.

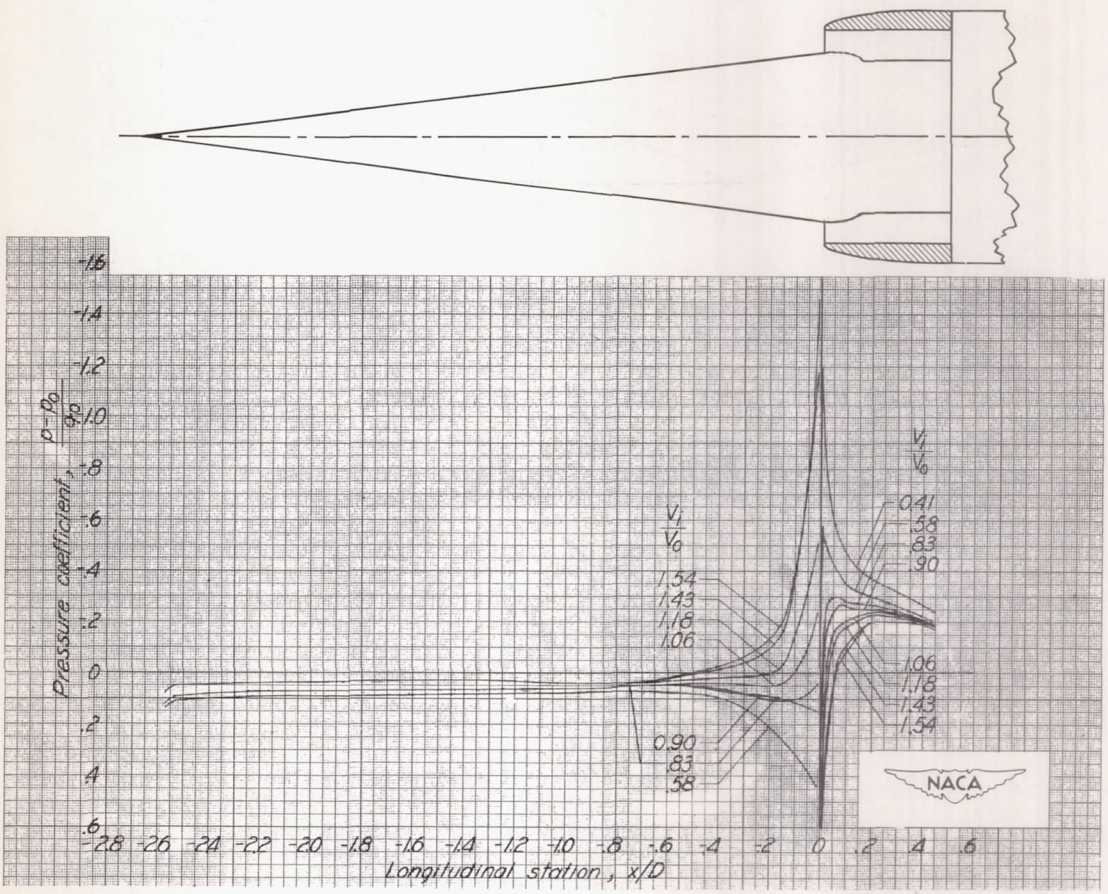

(b) $\alpha = 0^{\circ}$.

Figure 5.- Continued.

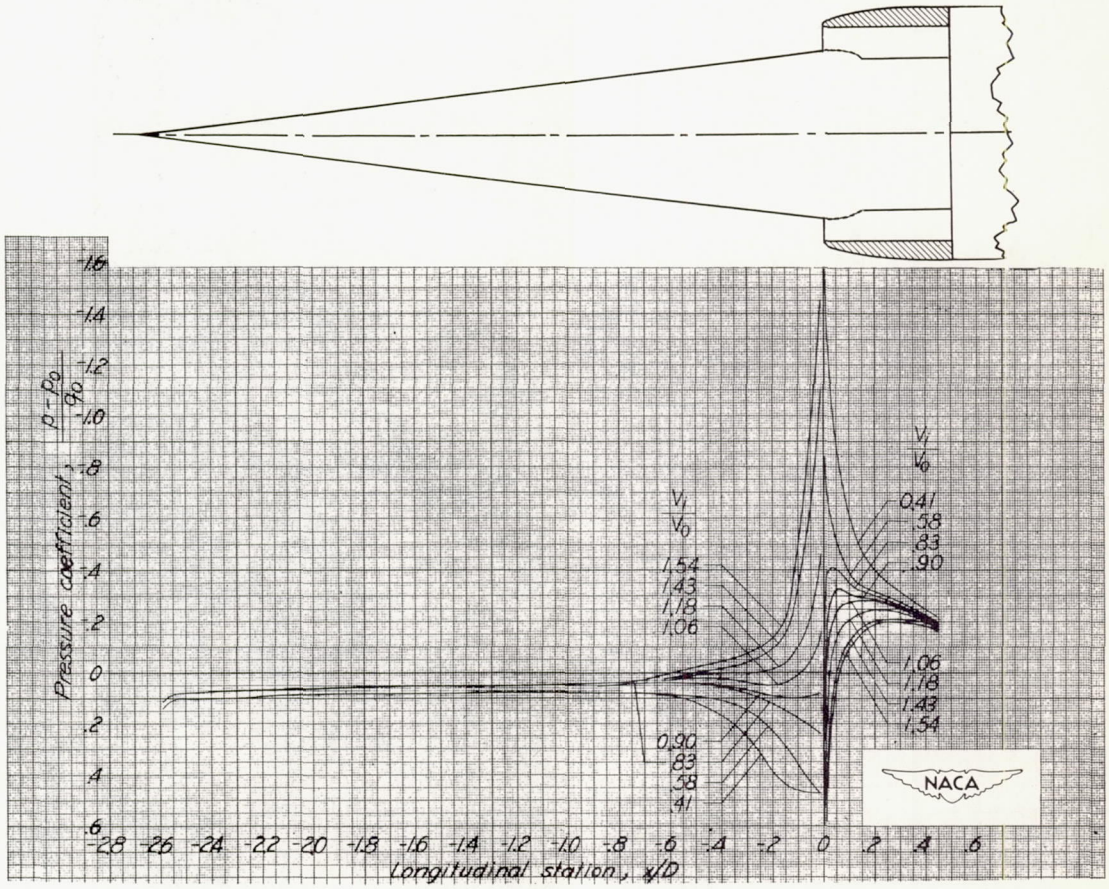

(c) $\alpha = 2^{\circ}$.

Figure 5.- Continued.

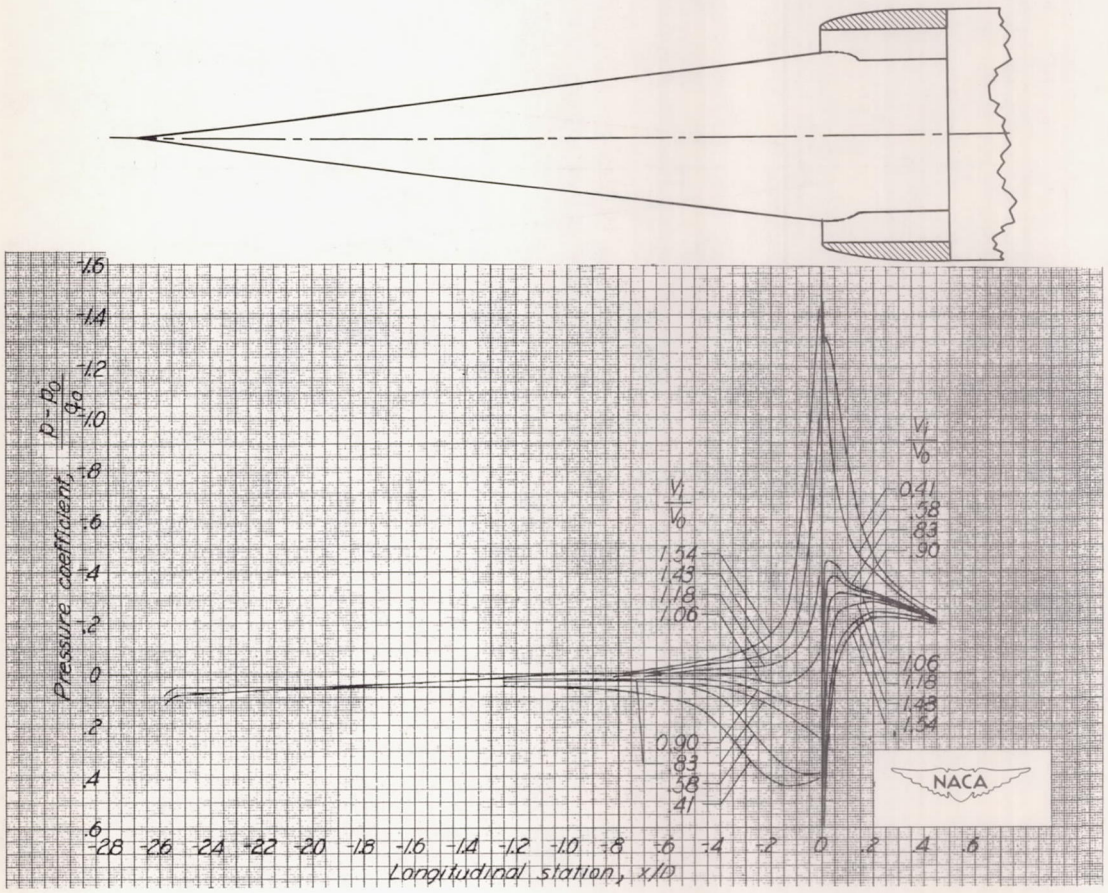

(d) $\alpha = 4^{\circ}$.

Figure 5.- Continued.

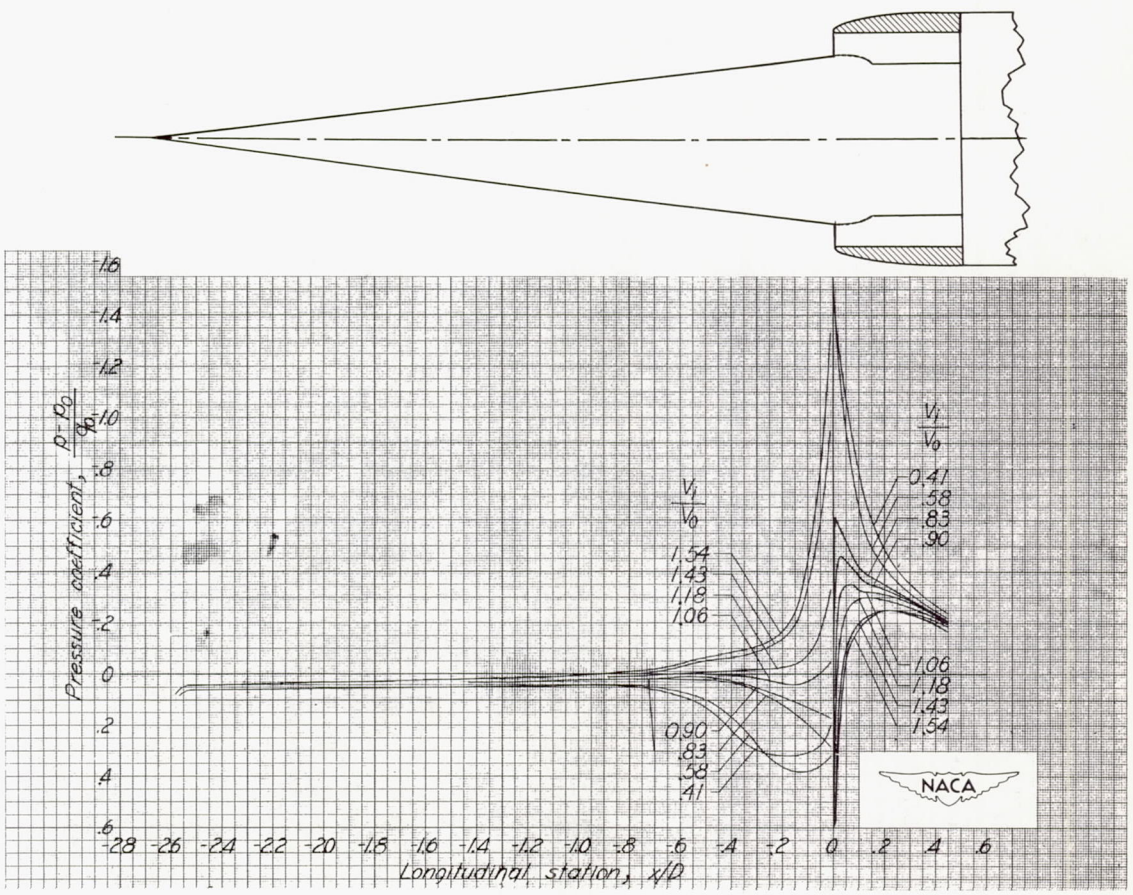

(e) $\alpha = 6^\circ$.

Figure 5.- Concluded.

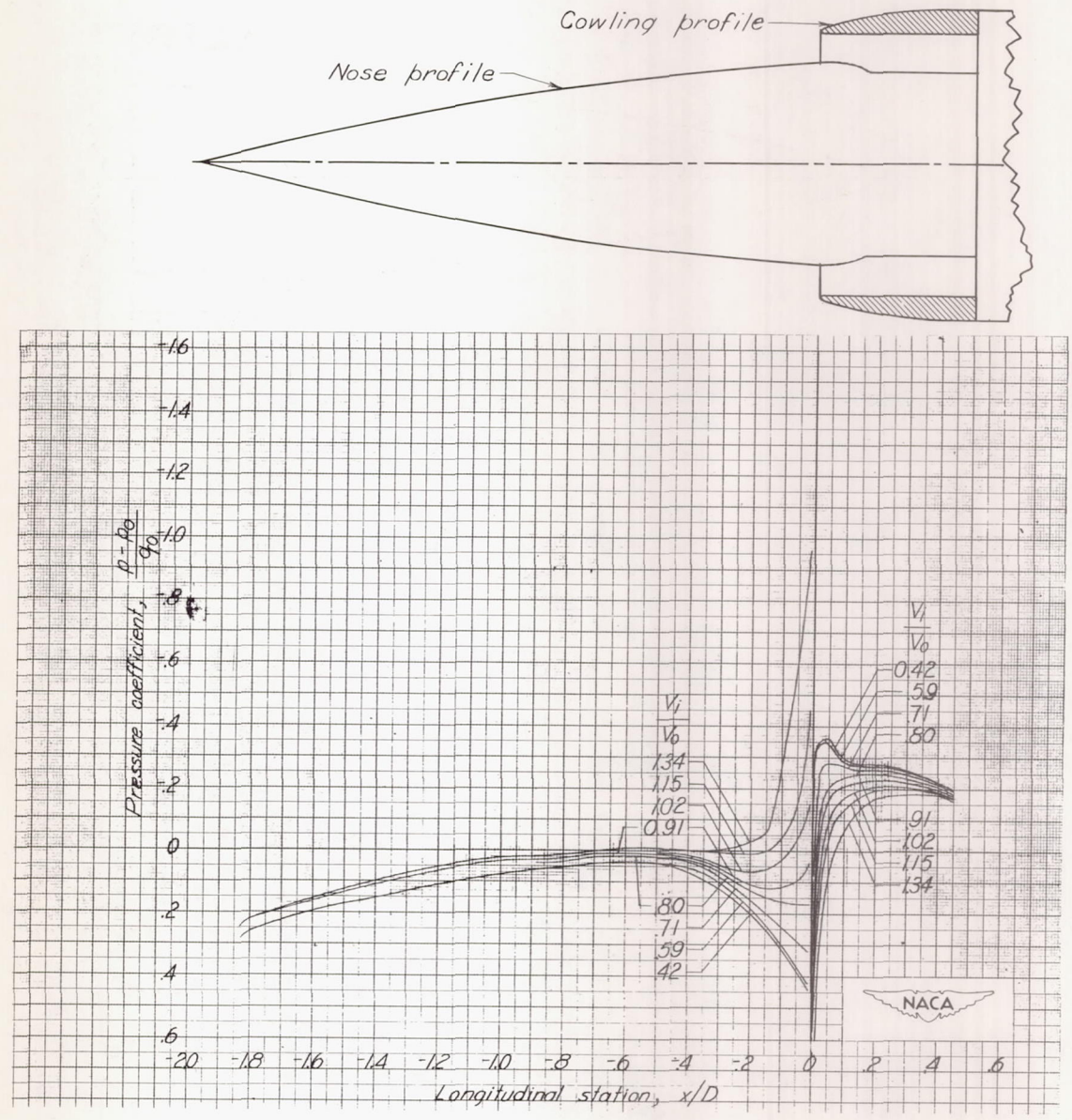

(a) $\alpha = -2^\circ$.

Figure 6.- Static-pressure distributions over top external surface of model with curved nose installed.

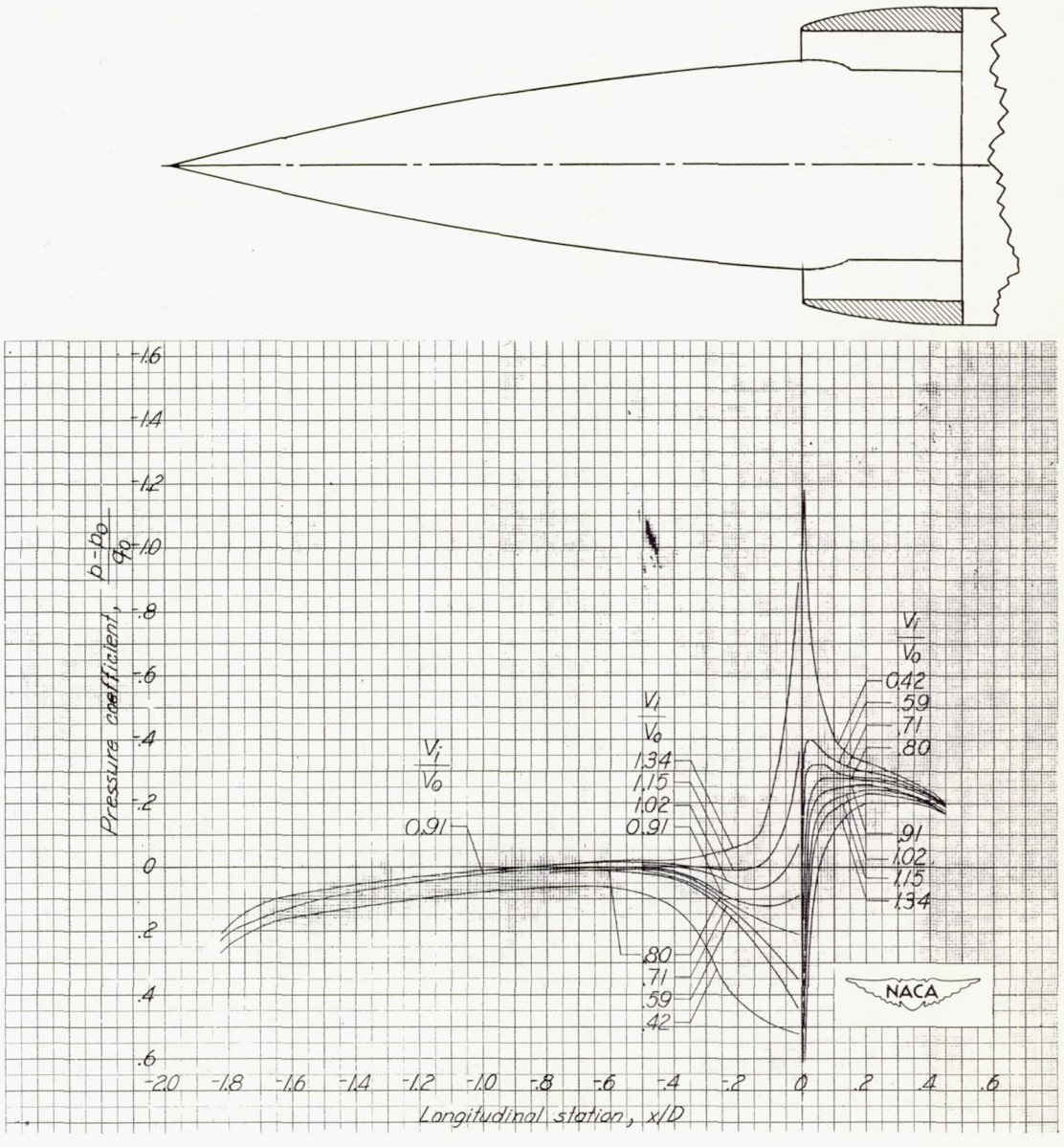

(b) $\alpha = 0^{\circ}$.

Figure 6.- Continued.

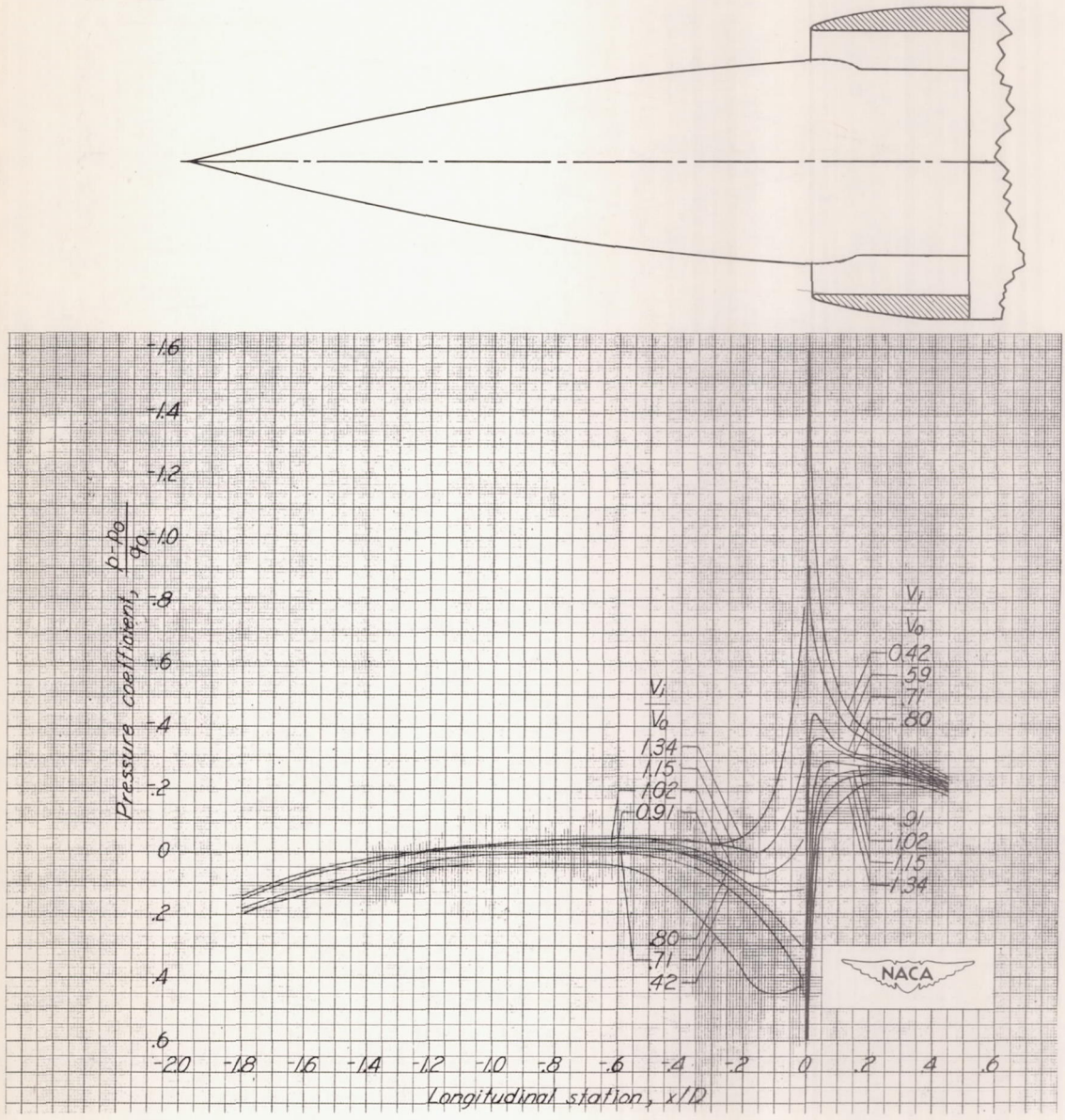

(c) $\alpha = 2^{\circ}$.

Figure 6.- Continued.

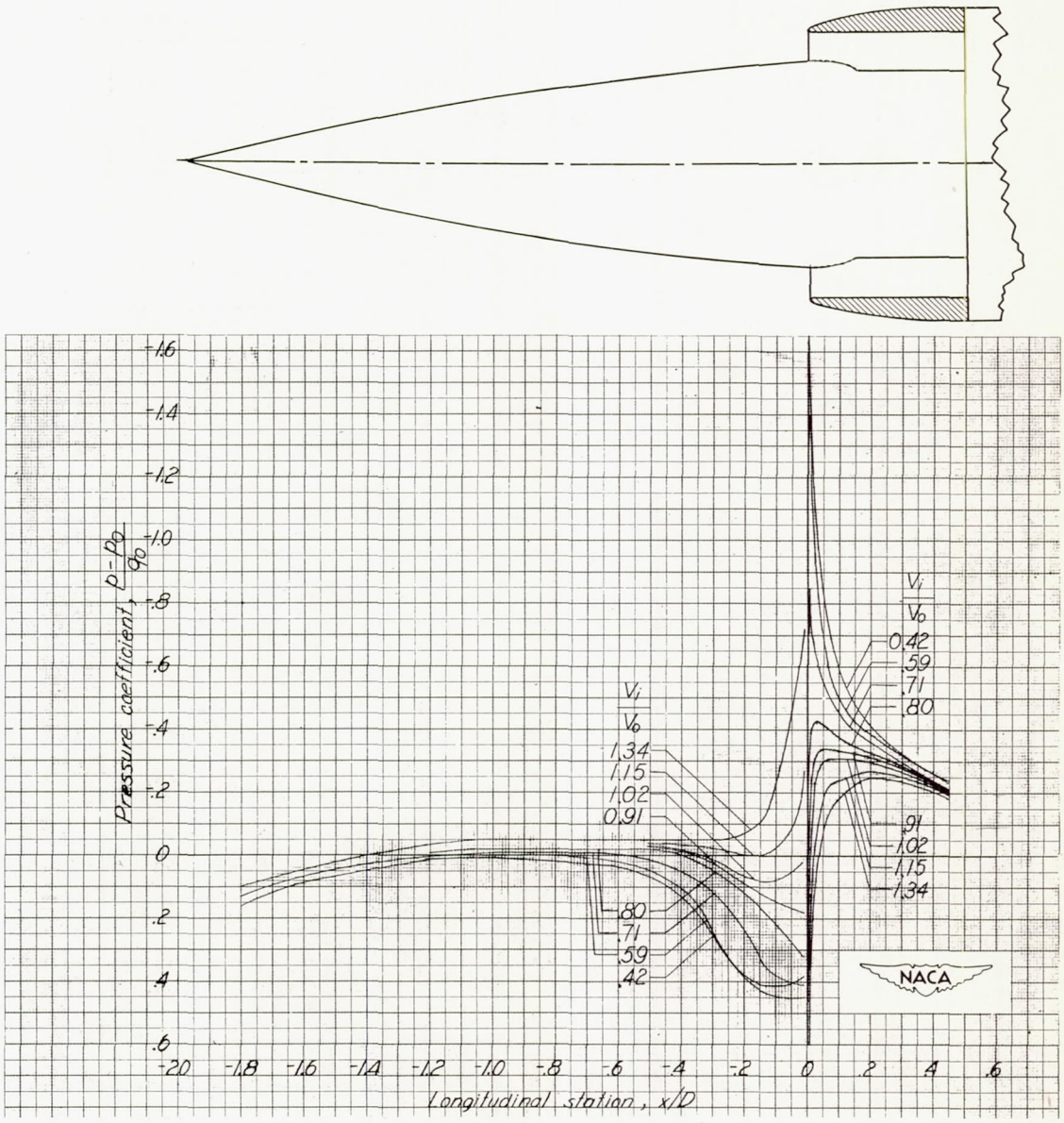

(d) $\alpha = 4^\circ$.

Figure 6.- Continued.

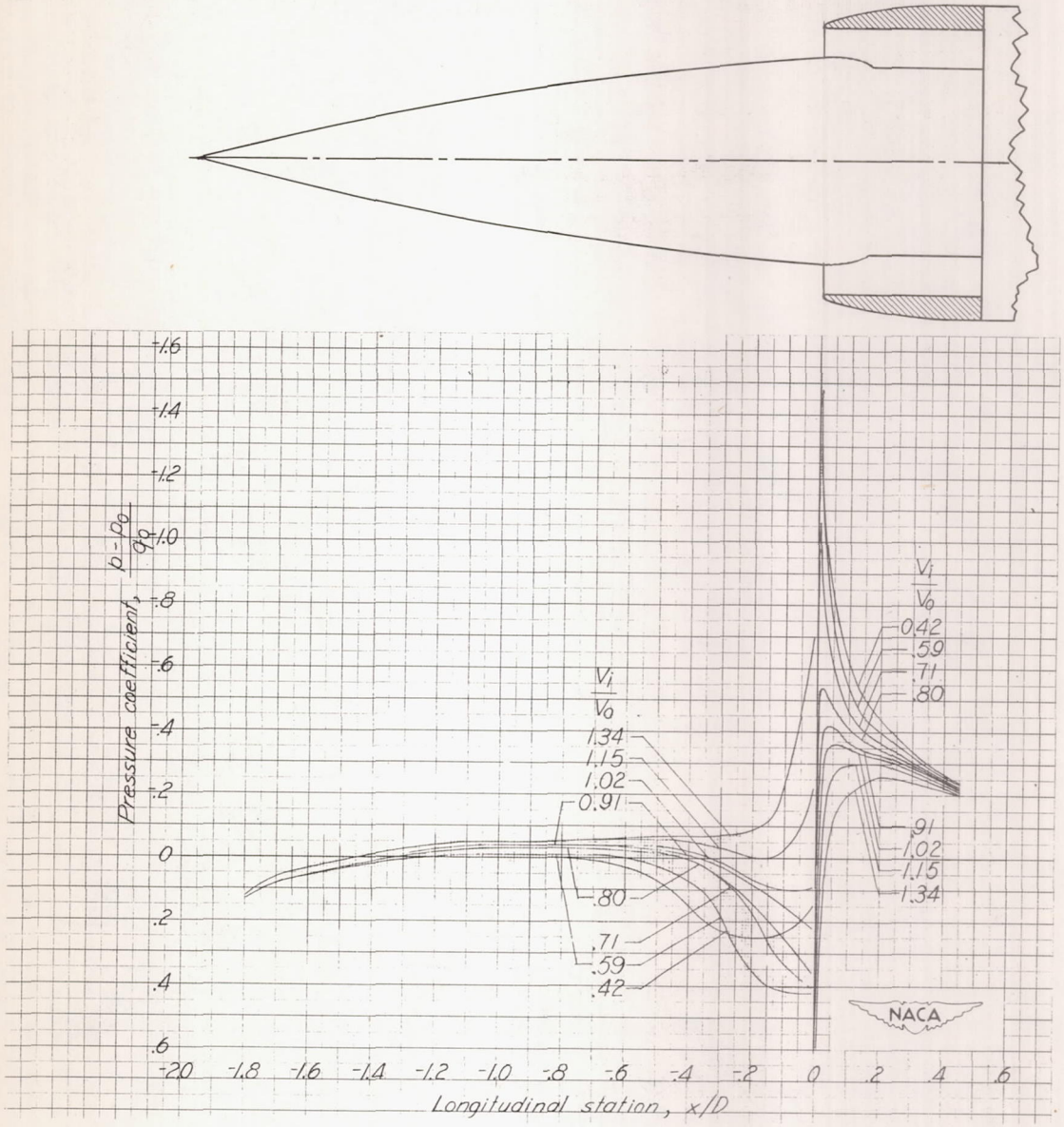

(e) $\alpha = 6^{\circ}$.

Figure 6.- Concluded.

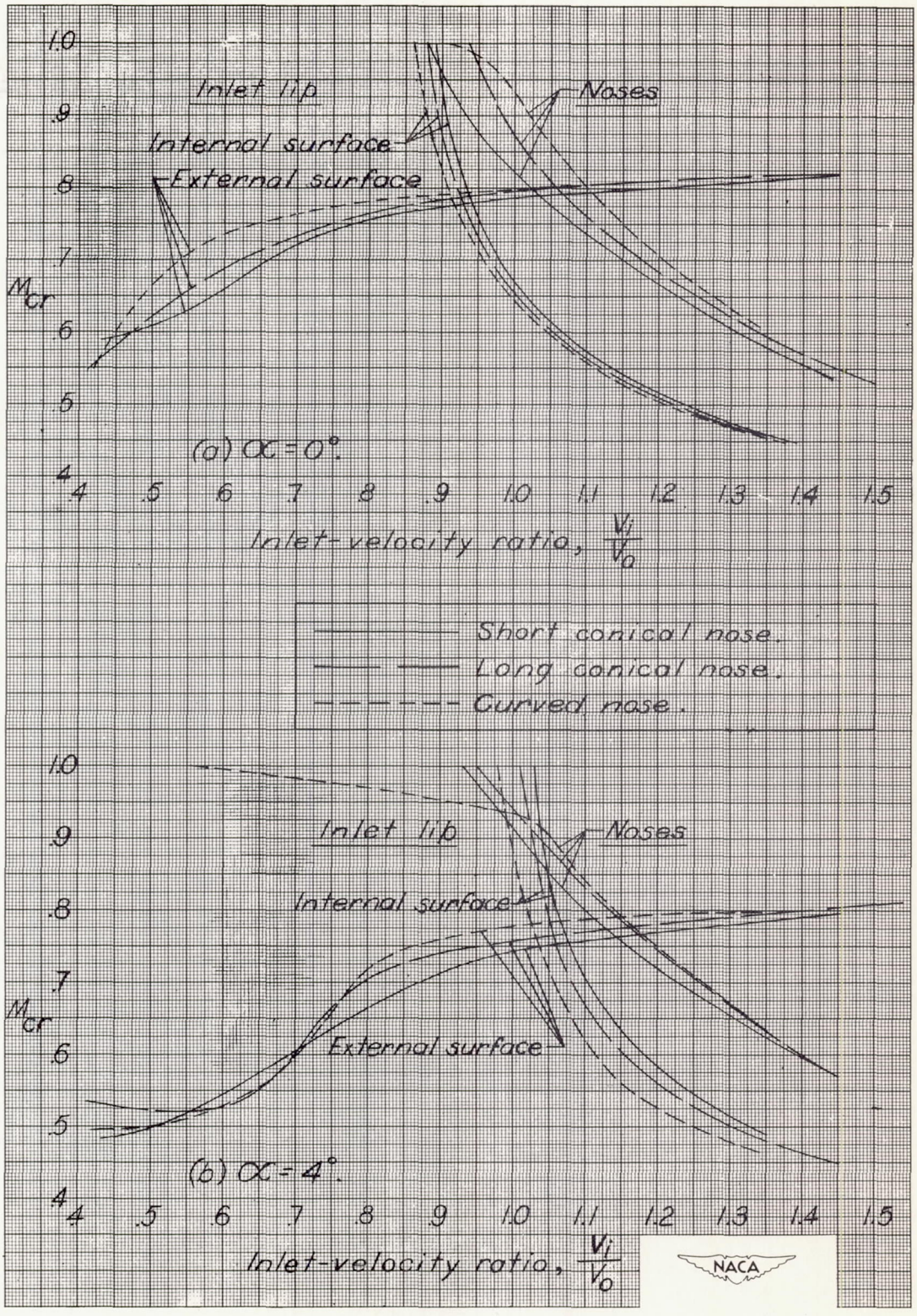

Figure 7.- Predicted critical Mach number characteristics of top surfaces of the annular inlet configurations.

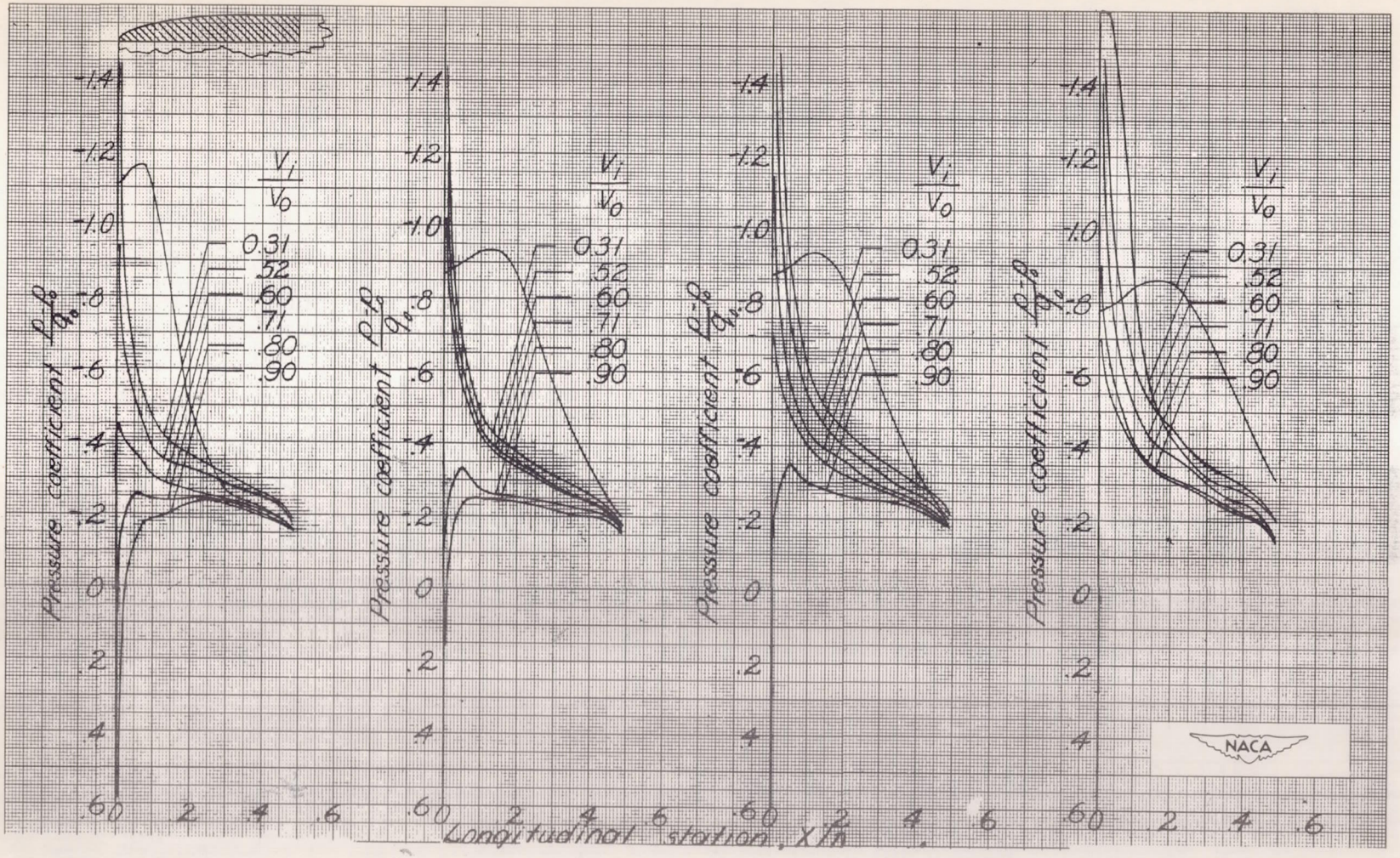

(a) $\alpha = 0^\circ$. (b) $\alpha = 2^\circ$. (c) $\alpha = 4^\circ$. (d) $\alpha = 6^\circ$.

Figure 8.- Static-pressure distributions over top external surface of the NACA 1-85-050 open-nose cowling.

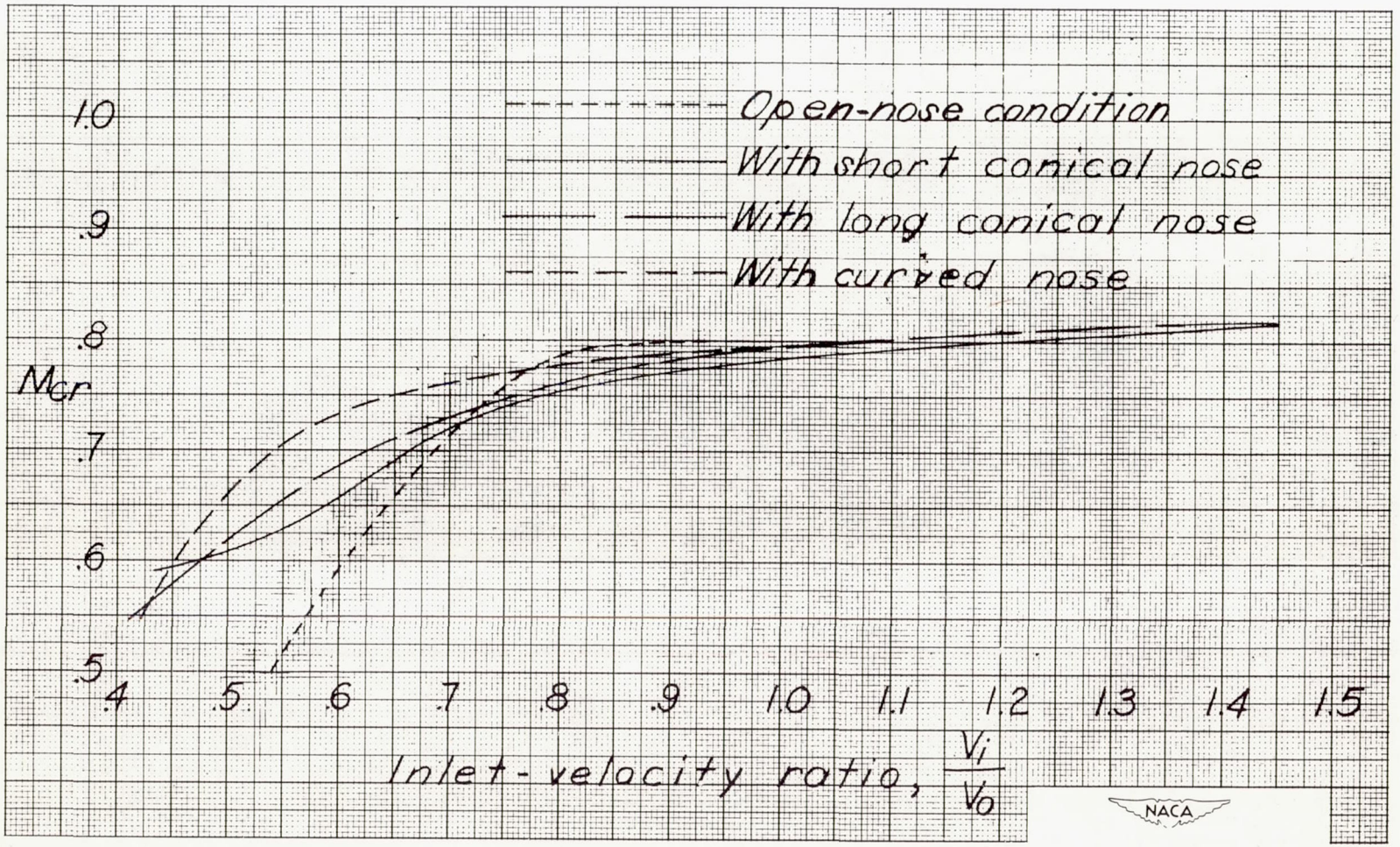

Figure 9.- Effect of noses on critical Mach number characteristics of external surface of lip of NACA 1-85-050 cowling. $\alpha = 0^{\circ}$.

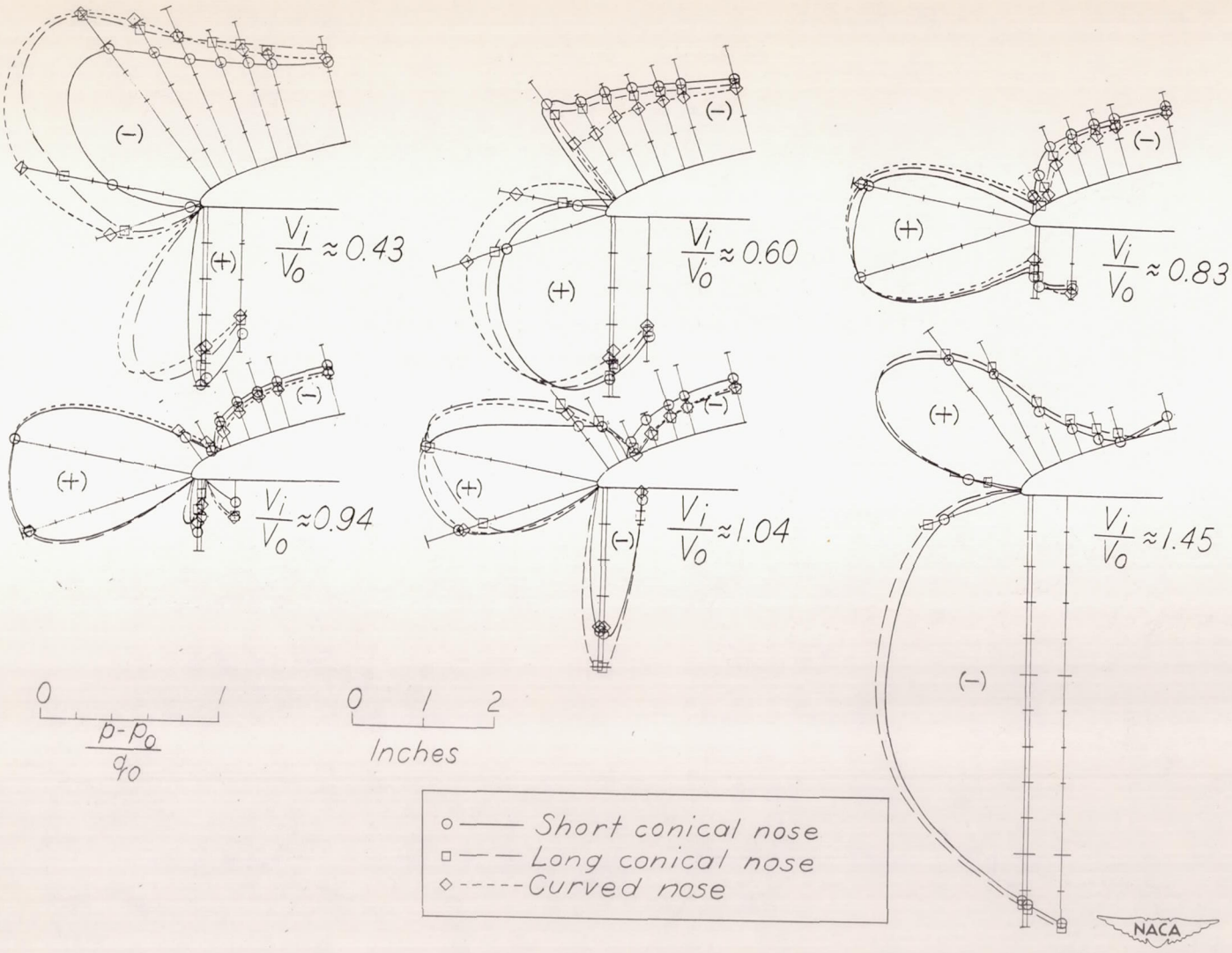

(a) $\alpha = 0^\circ$.

Figure 10.- Static-pressure distributions around top section of lip of NACA 1-85-050 cowling with the three noses installed.

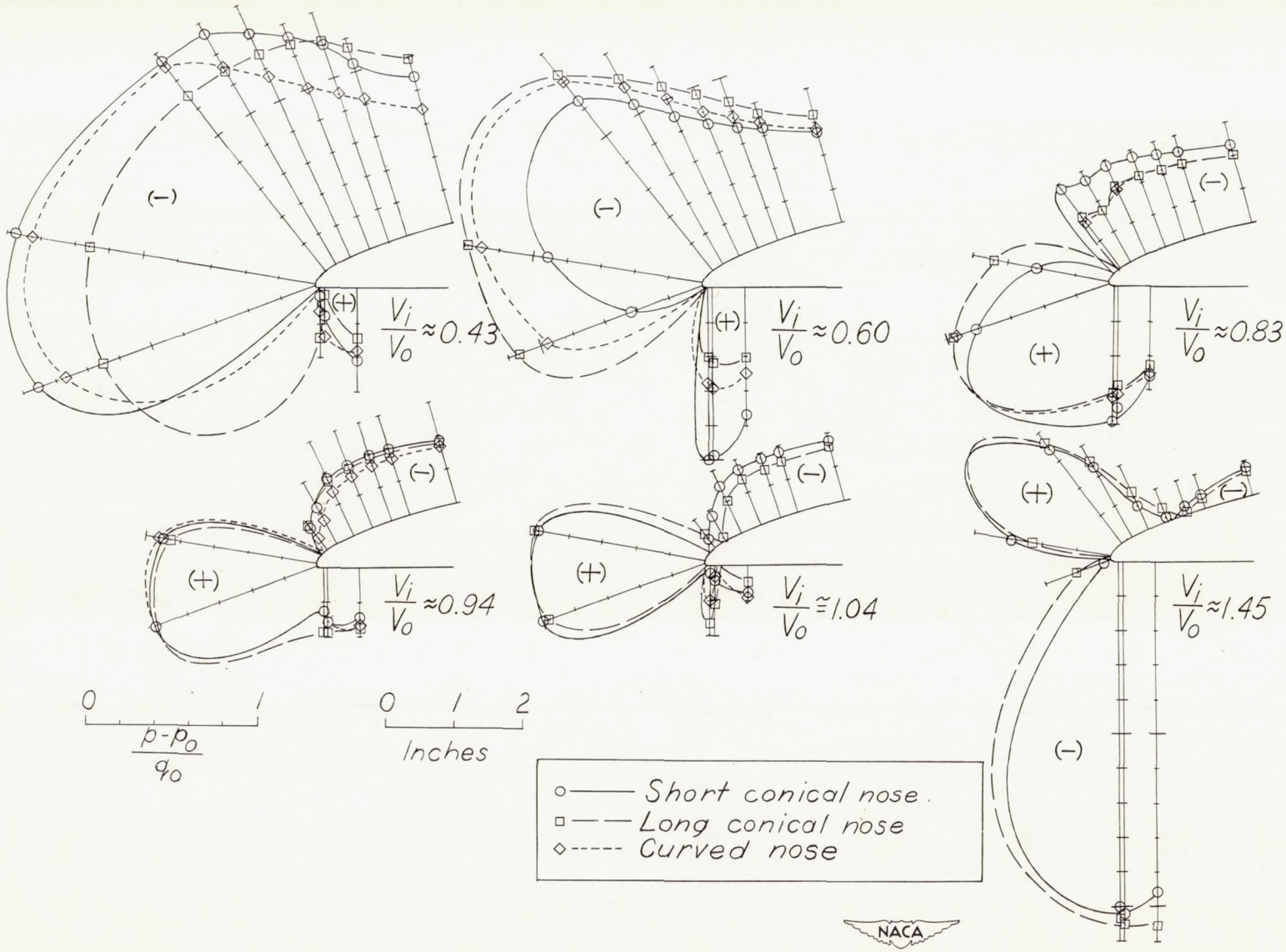

(b) $\alpha = 4^\circ$.

Figure 10.- Concluded.

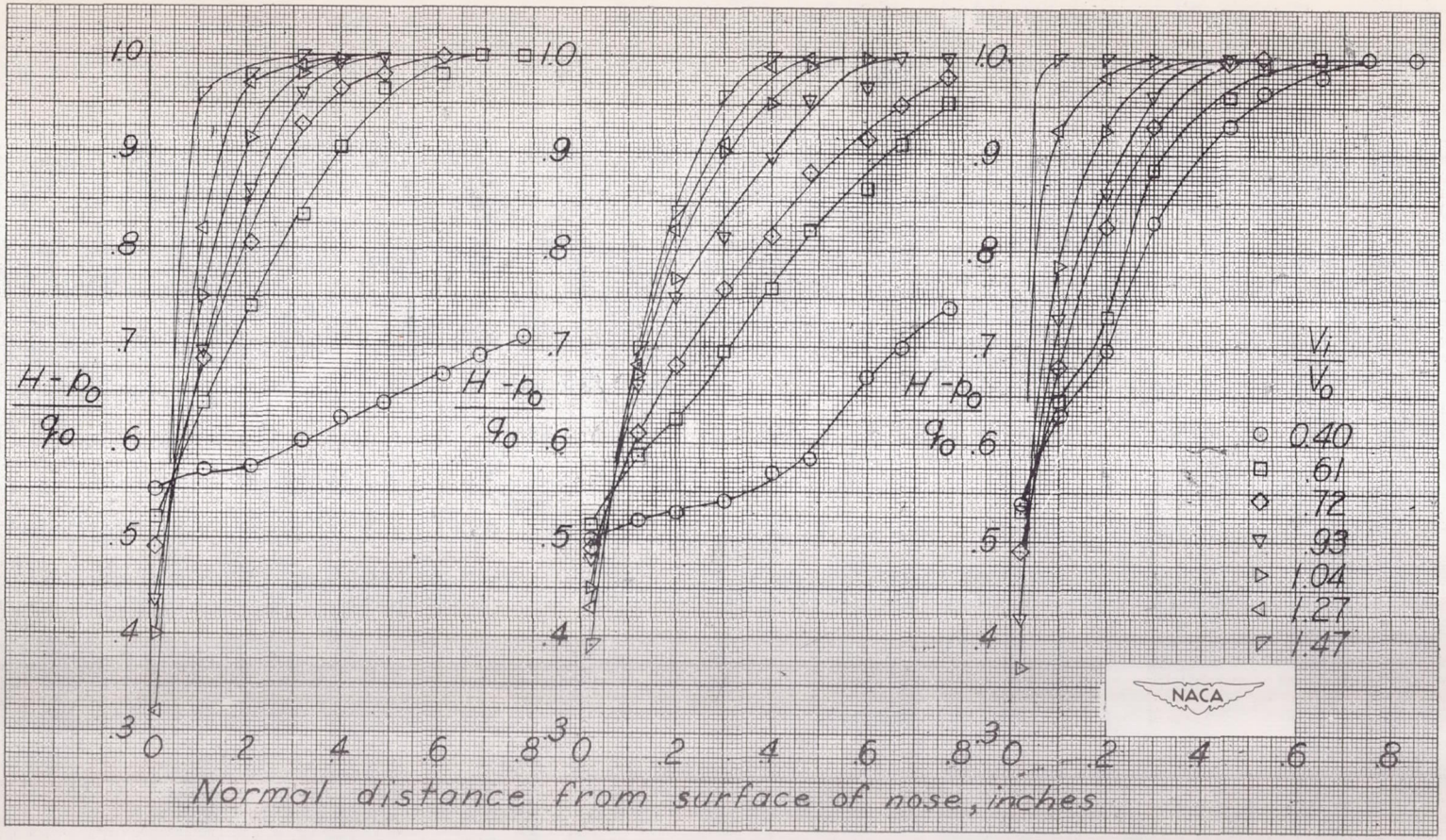

(a) Short conical nose. (b) Long conical nose. (c) Curved nose.

Figure 11.- Total-pressure distributions in the boundary layers of the three noses at the inlet. $\alpha = 0^\circ$.

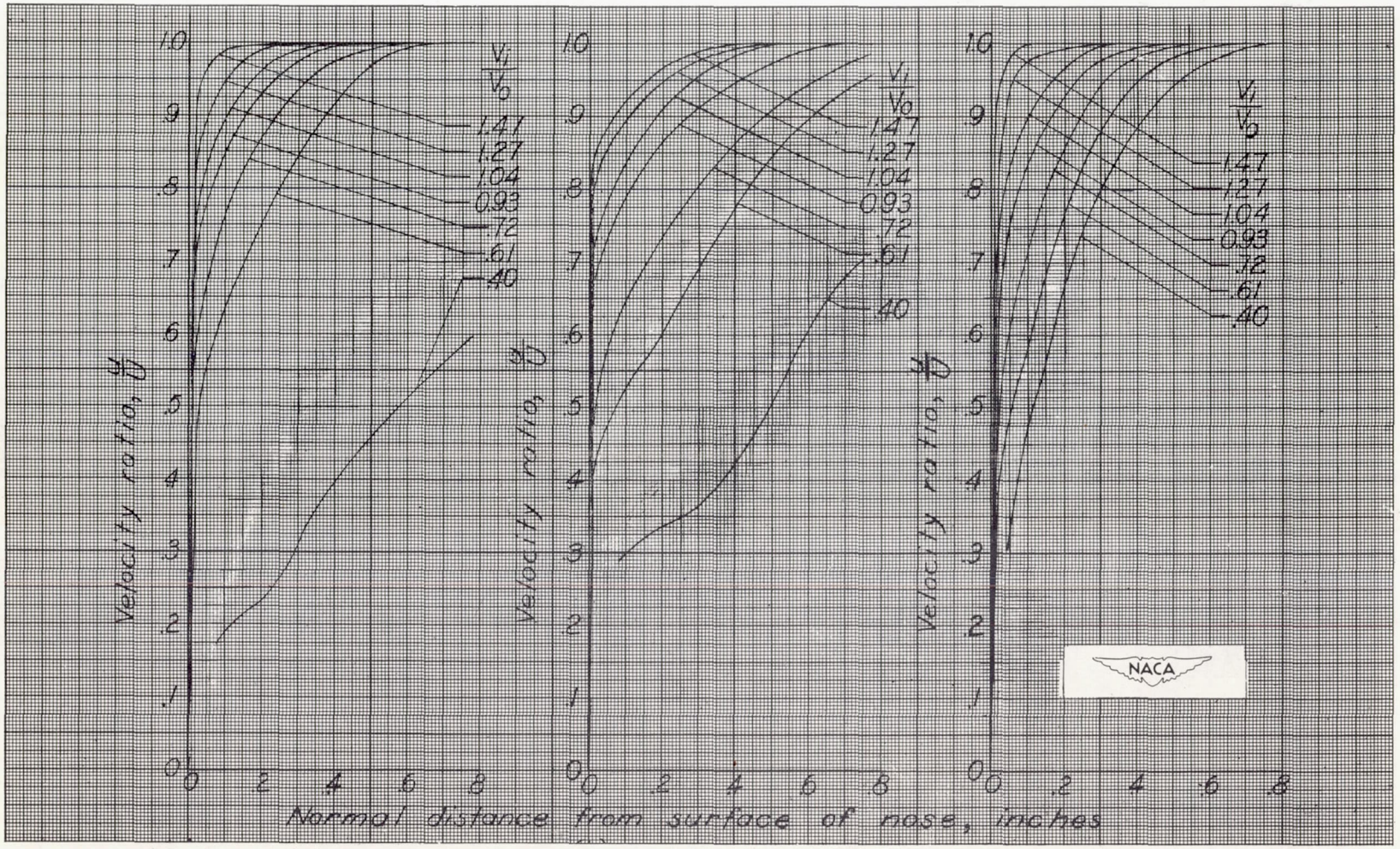

(a) Short conical nose. (b) Long conical nose. (c) Curved nose.

Figure 12.- Velocity distributions in the boundary layers of the three noses at the inlet. $\alpha = 0^{\circ}$.

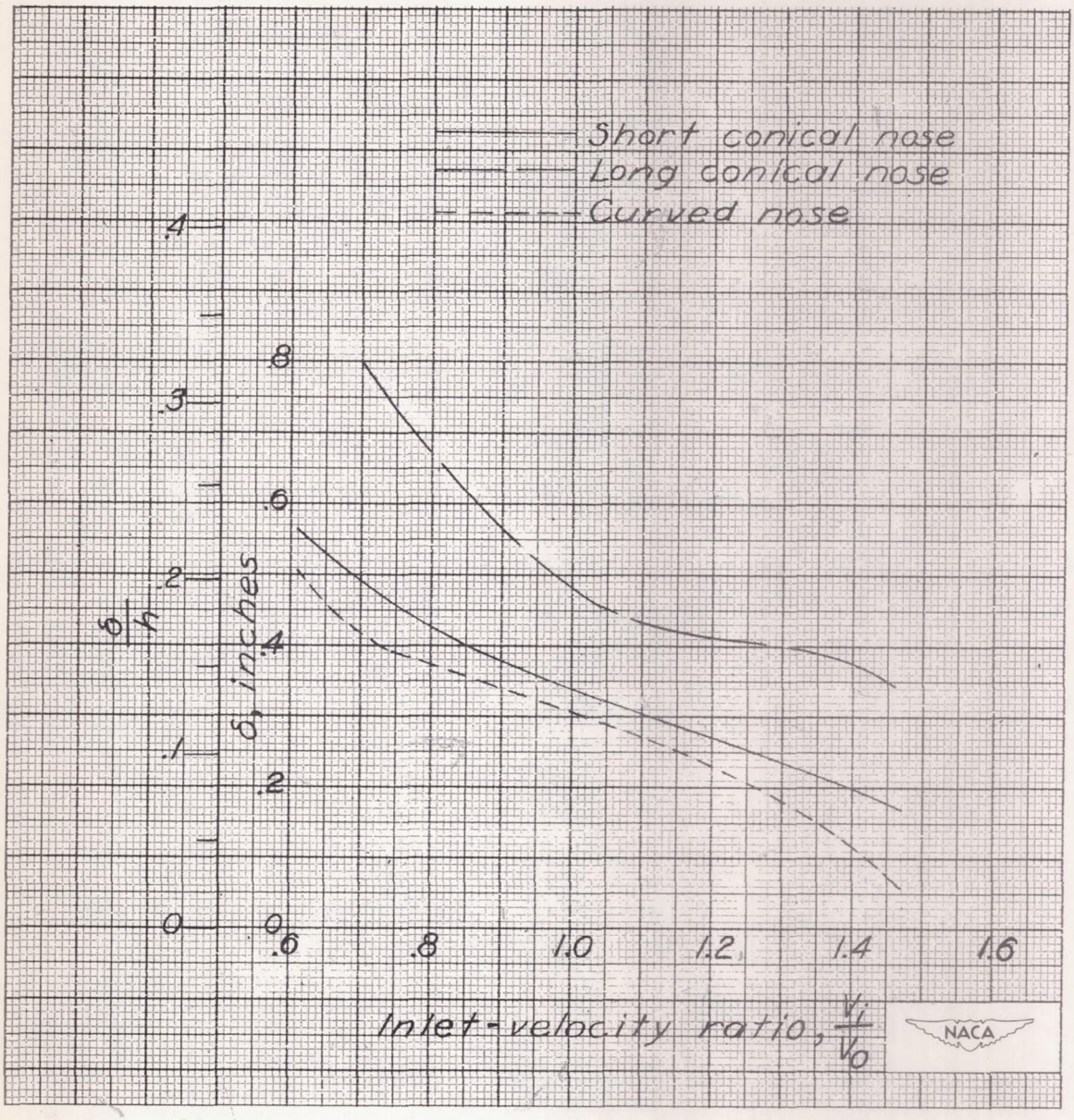

Figure 13.- Boundary-layer thickness on the three noses at the inlet as a function of inlet-velocity ratio. $\alpha = 0^{\circ}$.

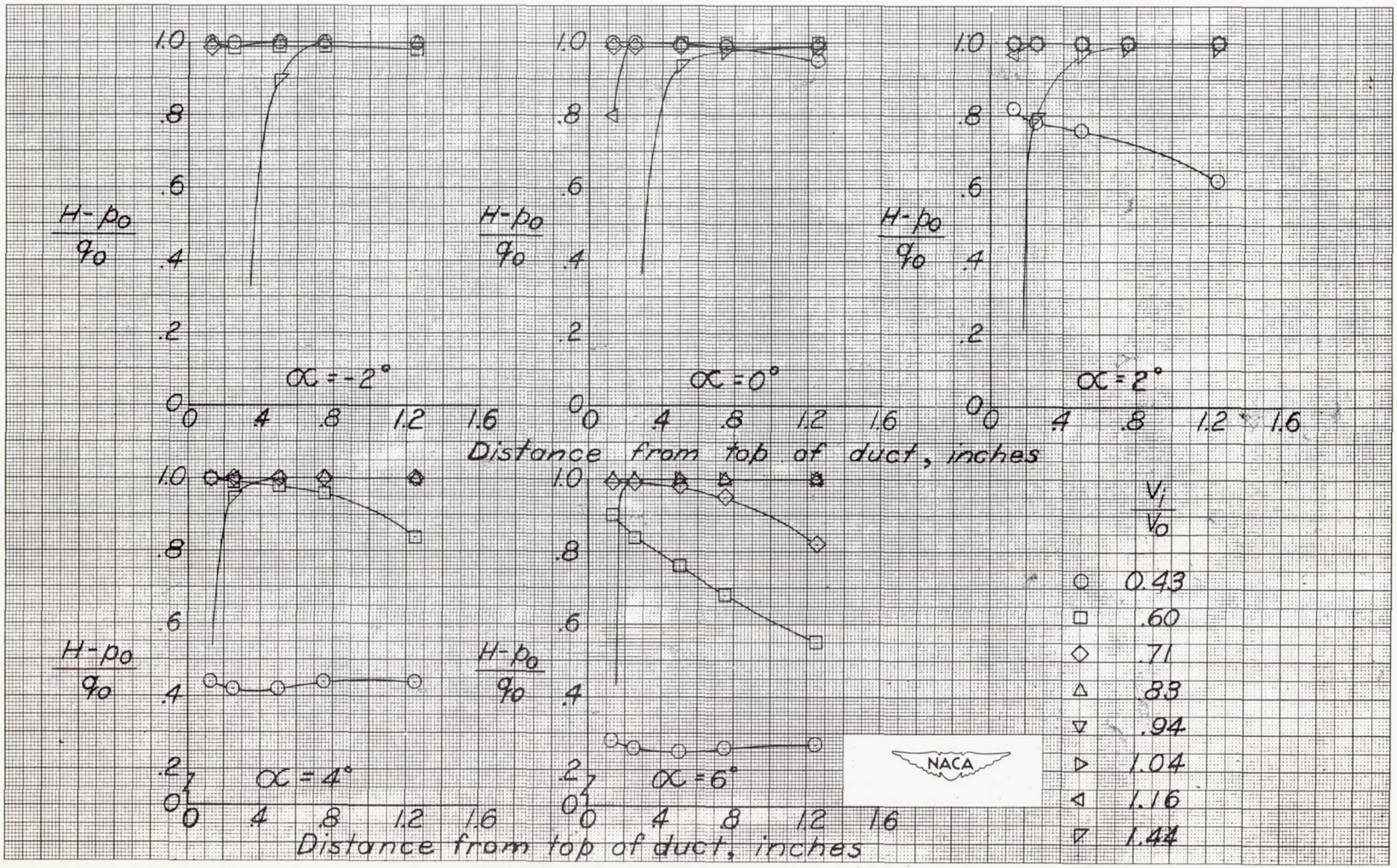

(a) Short conical nose.

Figure 14.- Total-pressure recoveries in the outer half of the inlet annulus at the top of the model. Station 0.75.

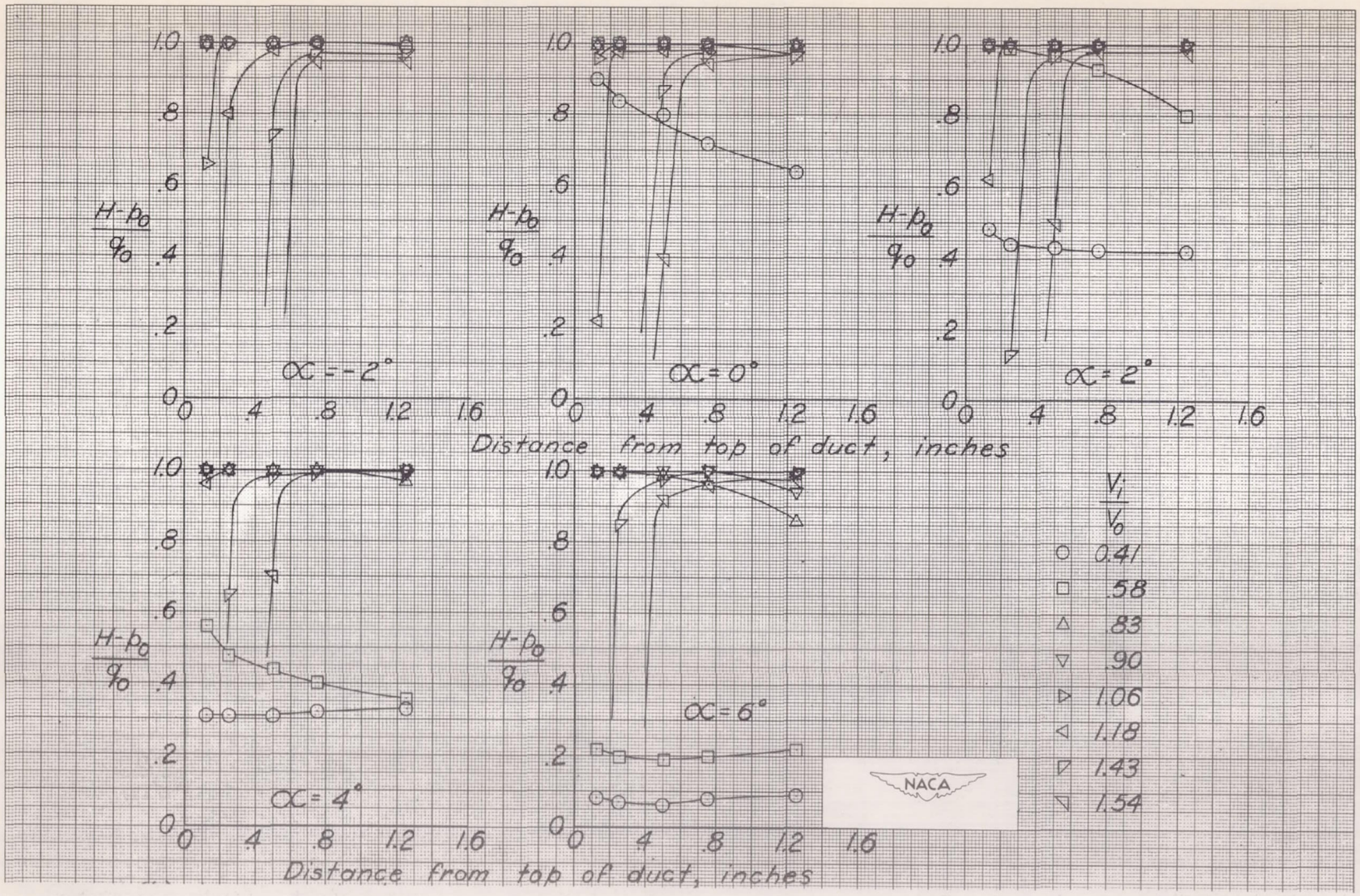

(b) Long conical nose.

Figure 14.- Continued.

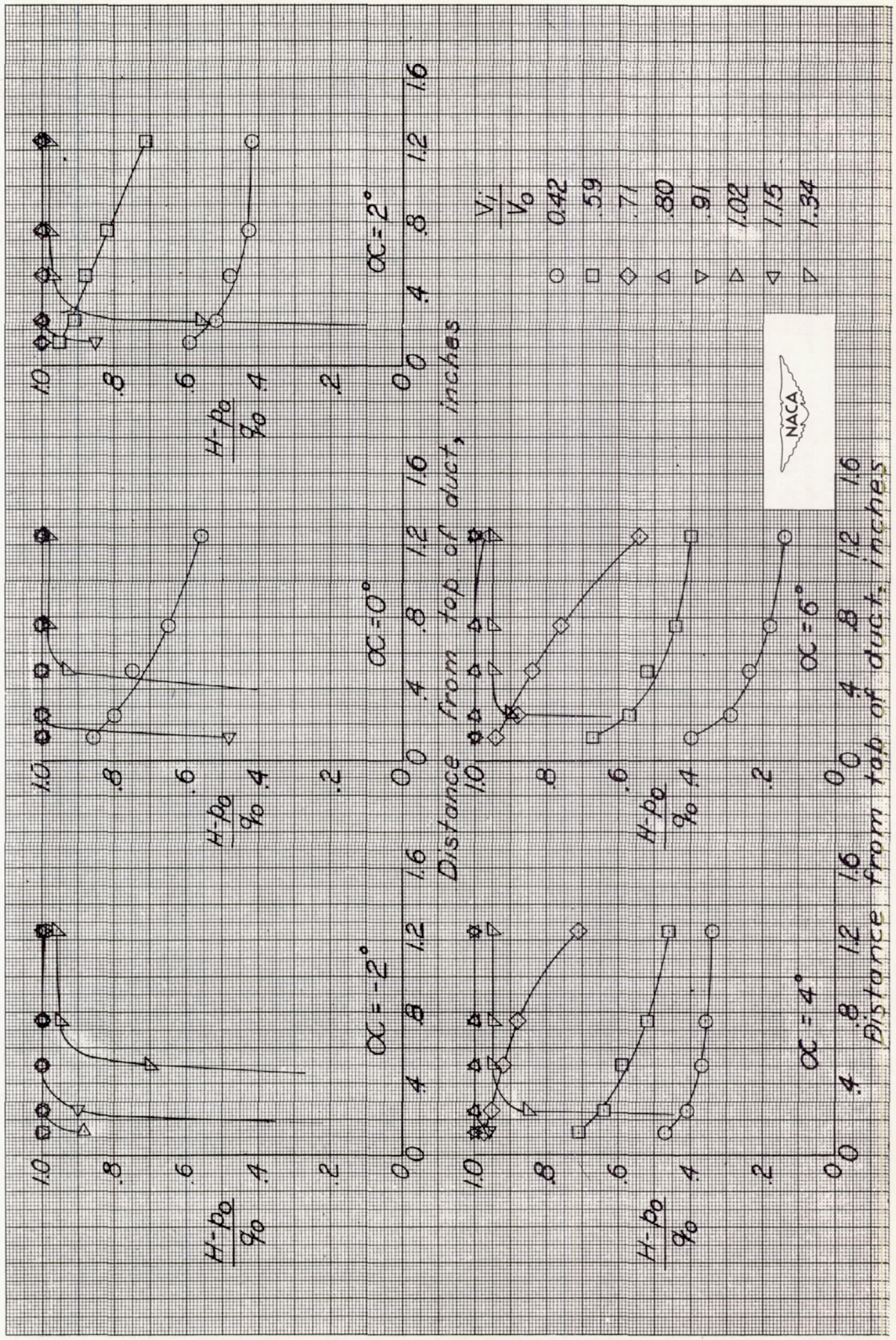

(c) Curved nose.

Figure 14.- Concluded.